RSC Advances

ROYAL SOCIETY OF CHEMISTRY

www.rsc.org/advances

Journal Name

Dynamic Article Links ►

Cite this: DOI: 10.1039/c0xx00000x

www.rsc.org/xxxxxx

ARTICLE TYPE

A Review on Materials for Light Scattering in Dye-sensitized Solar Cells

T. G. Deepak, G. S. Anjusree, Sara Thomas, T. A. Arun, Shantikumar V Nair, A. Sreekumaran Nair*

Keywords: DSCs, Metal Oxides, Active Layer, Scattering Layer, Mie theory.

Dye-sensitized solar cells (DSCs) offer interesting possibilities in photovoltaics which is the technology of harvesting solar photons to generate electricity. Improving the charge transport through the metal oxide film, finding dyes with better absorption both in the visible and near IR regions of the solar spectrum and fabricating innovative materials for scattering layer are the proposed way forward for improving the efficiency of DSCs. Light scattering is employed in dye-sensitized solar cells to improve the optical absorption of the incident light. The conventional method of light scattering in DSCs is by using a separate scattering layer consisting of large particles with diameters comparable to the wavelength of the incident light. An additional over-layer on nanocrystalline TiO_2 photoanode will encourage light scattering in DSCs especially in the red part of the solar spectrum. Different nanostructures with good dye adsorption and light scattering properties were tried as light scattering layers in DSC. Of late, scientists attempted the use of functional materials having enhanced light scattering properties and high internal surface area as dual function materials (that is a single layer of material capable of both light absorption and scattering). This review explores theoretical aspects and materials innovation for light scattering and their application in DSCs.

Contents

1. Introduction

The dye-sensitized solar cells (DSCs) have become one of the promising solar cells to convert solar energy to electricity with good efficiency at considerably low fabrication cost.[1] A dye-sensitized semiconductor coated on a glass substrate is the heart of a DSC system. The TiO_2 semiconductor film with 10-15 μm thickness is used as the active layer in a DSC photoanode. A platinum (Pt)-coated counter electrode is sandwiched with photoanode and the space between the electrodes is filled with a liquid electrolyte that contains I-/I3- redox couple. Solar radiation generates electrons from dye molecules and transfer them to the external circuit through the semiconductor oxide network.

The research on DSCs for higher conversion efficiency is intensively pursued by different research groups around the globe. The current focus is mainly on the modification of dyes, electrolyte and the semiconductor oxides for a better performance. The conventionally used dyes absorb only in the visible region of the solar spectrum. The dyes with broader absorption of solar spectrum such as Black dye are preferred in DSCs. The iodide/triiodide electrolyte offers excessive driving force of 0.6 eV for dye regeneration which leads to a potential drop of about 600 mV. This is one of major drawbacks of iodide/triiodide electrolyte and the limiting factor for increasing the conversion efficiency further from the current level. The organic solid hole-transport material (HTM) is considered as best alternative to the liquid electrolytes to obtain a high V_{oc} of 986 mV. [2] But penetration of this material into nanoporous film is one of the major drawbacks of the HTMs. The morphology of TiO_2 in the photoanode film plays a vital role in determining the conversion efficiency.[3-6] One can employ one-dimensional (1D) nanostructures to provide direct pathway for electron diffusion. Using nanostructures promoting enhanced light scattering is yet another possible way to enhance the conversion efficiency.

The idea of light scattering in DSCs is to extend travelling distance by confining light propagation within the photoanode. This strategy will promote interaction of incident photons with the dye molecules. As working electrode is normally made up of TiO_2 nanoparticles of 10-25 nm size, it remains transparent to the visible region of solar spectrum. In this scenario, solar energy is only partially harvested by the active layer. Inclusion of large particles of size comparable to the wavelength of incident light encourages better light scattering in DSCs especially from the red part of the solar spectrum. The efficiency decrement of DSCs when scaling up to larger modules is a notorious problem. Light scattering layer approach is an effective and practical method to enhance efficiency in larger DSC modules and solar panels, though this is technologically challenging and expensive. Grätzel et al. have reported a conversion highest efficiency of 12.3% with porphyrin-sensitized solar cells using cobalt (II/III)-based electrolyte.[2a] Here they had incorporated a 5 μm thick light scattering layer (~ 400 nm sized TiO_2 particles) over 5μm thick active layer. Recently the same research group has reported 13% efficiency with molecularly engineered porphyrin dye.[2b] Chiba et al. had achieved a highest certified conversion efficiency of 11.1 % by incorporating light scattering layer.[7] This is the highest conversion efficiency tested by any of public test center (National Institute of Advanced Industrial Science and Technology, AIST, Japan).

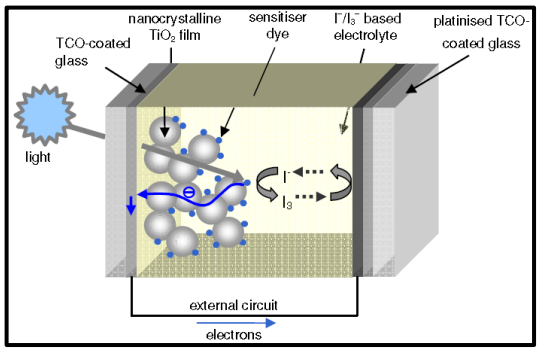

Fig.1 Schematic of liquid electrolyte Dye sensitized solar cell.[8]

This review article presents theoretical background on light scattering and outlines recent developments in the light scattering approach to enhance current density and power conversion efficiency of DSCs. We believe the review is topical and will be interesting to the scientists working in the same and related fields.

2. Operational principle of DSCs

A mesoscopic semiconductor oxide in contact with the redox electrolyte or hole-conductor is the major part of DSC.[8] In **Fig 1**, schematic of dye sensitized mesoporous nanoparticles in contact with the liquid electrolyte is shown. TiO_2 (anatase) has been widely employed as the semiconductor oxide although wide band-gap materials such as ZnO and Nb_2O_5 have also been experimented. A monolayer of sensitizer is attached to the nanocrystalline particles in the film. Electrons from dye are injected into the conduction band of the semiconductor oxide by photoexcitation. Dye is regenerated by the organic electrolyte containing a redox couple (iodide/triiodide couple). Iodide is responsible for dye regeneration; in turn iodide is regenerated by reduction of triiodide at the counter electrode. The voltage generated under illumination is the difference between quasi Fermi level of the semiconductor oxide and the redox potential of the electrolyte.

The high surface area of semiconductor oxide is critical for the high performance of DSCs. Since the dye monolayer is adsorbed on the semiconductor oxide; it is obvious that its high surface area will enhance the light absorption. The function of mesoporous semiconductor oxide is similar to the thylakoid vesicles in green leaves. [9] The use of mesoporous film enhances the interfacial surface area over the geometrical surface area by 1000 fold

CREATED USING THE RSC ARTICLE TEMPLATE (VER. 3.0) - SEE WWW.RSC.ORG/ELECTRONICFILES FOR DETAILS

ARTICLE TYPE

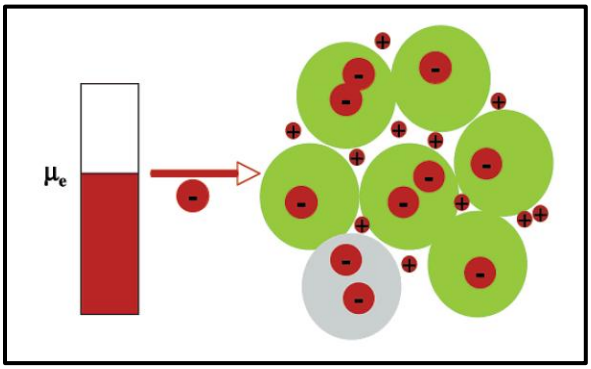

Fig.2 Local screening of electrons into nanocrytalline film. μ_e is Fermi level of the electrons.[9]

for a 10 μm thick film. Hence, when light passes through mesoporous structure, it intersects hundreds of dye monolayers. Moreover, the semiconductor oxide also fulfills the role of electron conduction.

A wide band-gap semiconductor oxide film acts as an insulator in dark. A single electron injection in a 20 nm-sized particle generates an electron concentration of 2.4×10^{17} cm^3.[8] Fermi level of semiconductor oxide should be close to the conduction band for the undeterred flow of electrons. Otherwise there is a certain probability of trapping of electrons which affects the diffusion coefficient. As shown in **Fig 2**; the injected electron can be screened by the cations in surrounding electrolyte which results in electron percolation. [10] Consider a 10 μm thick mesoscopic film composed of 20 nm sized particles. Beer-Lambert's law explains light absorption in terms of the reciprocal length.

$$\alpha = \sigma c \qquad (1)$$

where α is the optical absorption cross-section of the sensitizer, σ is the sensitizer's concentration in the mesoporous film and c is the velocity of the light.
The light harvesting efficiency (LHE) given by

$$LHE(\lambda) = 1 - 10^{-\alpha d}, \qquad (2)$$

where d is the thickness of the film.
Incorporation of 100-400 nm sized anatase particles enhances the light absorption in the near-infrared (N-IR) region of the solar spectrum.

2.1 Dynamic competition in DSC

Dynamic competition between the electron transfer, charge-transport processes and several loss pathways determine the quantum yield of DSCs.
Different loss pathways are listed below:

- Decay of the excited dye.
- Charge recombination of injected electrons with dye cations and with the redox electrolyte.

Dynamic competition between forward processes and loss path ways decides the efficiency of DSCs.

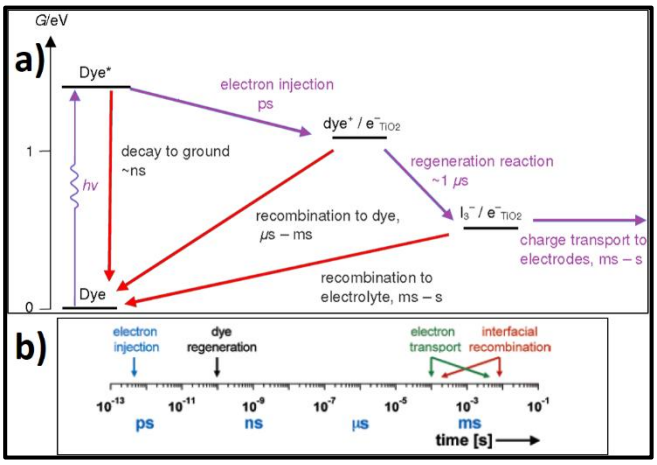

Fig.3a Forward processes (light absorption, electron injection, dye regeneration and charge transport) are indicated by violet arrows and loss paths (excited-state decay to ground and electron recombination with dye cations and oxidized redox couple) ways indicated by red arrows.[8] **b)** Schematic of time scale involved in different processes in DSC.[9]

Fig 3a&b show the dynamic competition processes in DSCs. Photoexcited electron has to be rapidly (in picoseconds) injected to the semiconductor oxide so that it cannot fall back into the ground state. The regeneration of dye (in ~ μs) should be faster than the feasible recombination with electrons in the oxide (passage time of electrons inside the oxide film must be lower than the exemplary time needed for them to recombine either with an oxidized dye molecule or electrolyte). The thicker nanoporous films cannot be used to increase the dye absorption because electrons are limited by diffusion path.

$$L_n = \sqrt{D_e \tau} \qquad (4)$$

where D_e and τ are diffusion coefficient and lifetime of electrons, respectively. For the successful collection, electron diffusion length must be greater than film thickness (d).

$$L_n > d \qquad (5)$$

Hence, an optimum thickness should be adopted for an efficient collection of electrons.

2.2 Incident Photon-to-Current-Conversion Efficiency

Incident photon-to-current-conversion efficiency (IPCE) or External Quantum Efficiency is described as the number of electrons (photocurrent) in external circuit divided by incident monochromatic photons.

$$IPCE(\lambda) = LHE(\lambda)\, \eta_{inj}\, \eta_{coll} \qquad (6)$$

CREATED USING THE RSC ARTICLE TEMPLATE (VER. 3.0) - SEE WWW.RSC.ORG/ELECTRONICFILES FOR DETAILS

ARTICLE TYPE

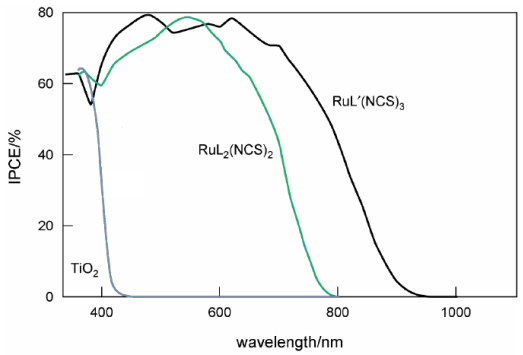

Fig.4 Spectral response of photocurrent for solar cell using different dyes. Violet color curve represents bare TiO_2; green and black represent N3 and Black dye, respectively. Here, L= 4, 4'-COOH-2,2' – bipyridine and L'= 4,4',4" –COOH-2,2': 6',2"–terpyridine [8]

LHE (λ) is the light harvesting efficiency for photons of wavelength λ; η_{inj} is quantum yield for electron injection from excited sensitizer into oxide semiconductor and η_{coll} is the collection efficiency of electrons to semiconductor oxide film.

2.3 Charge Injection

Sensitizer absorbs an energy which is greater than the HOMO-LUMO gap. An ideal sensitizer for photovoltaic cell should absorb all photons below a threshold wavelength of 920 nm. Functional groups such as carboxylate, hydroxamate, or phosphonate moieties must be incorporated to attach it to the nanoporous semiconductor film.[11] The energy level of the excited state should be matched with the lower edge of conduction band. It should be stable enough to run about 100 million turnover cycles (life time about 20 years in exposure to natural light). Ruthenium complexes known for their stability are commonly used as dyes in DSCs. *Cis*-Di (thiocyanato) bis (2,2'-bipyridyl) - 4,4'- dicarboxylate) ruthenium (II), known as N3 or N-719 dye depending on whether it carries four or two protons, was found to be a good solar absorber and charge-transfer sensitizer.[12] In 2001, Nazeeruddin et al. discovered a new dye, tri(cynato)-2,2'2"-terpyridyl-4,4'4"(tricarboxylate) Ru(II) ('black dye') competent with N3.[13] The spectral response of different dyes are shown in **Fig. 4**, where black dye shows a better performance over the others.

The photoexcitation ensures a shift in electron density from the ruthenium metal to the carboxylated bipyridyl ligand. The charge separation occurs from the π* orbitals of the ligand of ruthenium. Molecularly engineered sensitizers having injection times in the order of pico- or femtosecond range are also developed. [14-19] The injection is too rapid that it cannot redistribute its vibrational excitation energy by exchange with phonon in solids.

The quantum yield of charge injection (η_{inj}) indicates the fraction of photons absorbed by dye which are converted into electrons.

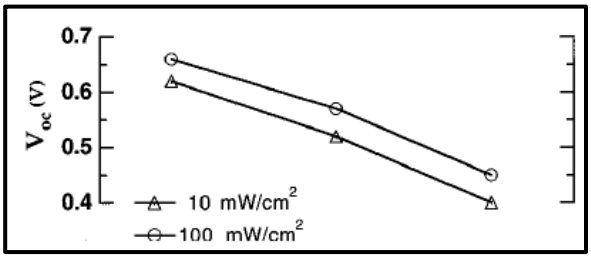

Fig.5 A graph plotted V_{oc} against ℓn $[I_3^-]$ at different radiant power.[38]

$$\eta_{inj} = k_{inj}/ (k_{deact}+k_{inj}) \quad (7)$$

k_{inj} is rate constant of injection of electron into oxide film, where k_{deact} represents rate constant of deactivation of the electronically excited state. To attain best η_{inj}, k_{inj} must be at least 100 times higher than k_{deact}.

2.4 Charge Separation and Recombination

A parameter k_b is introduced to characterize recombination rate. It is desirable to develop a sensitizer with high k_{inj} value and low k_b. The back reaction of electrons with oxidized ruthenium complexes involves a localized d orbital in the ruthenium metal. This energy loss channel is negligible because of the rapid reduction of ionized dye molecules by highly concentrated I^- ions.[20,21] An important parameter in limiting the conversion efficiency of DSCs is low photovoltage.[22] Charge recombination in nanocrystallite/redox electrolyte interface plays a significant role in reducing the photovoltage. Voltage determining recombination process is represented by the reaction,

$$2e^- + I_3^- \rightarrow 3I^- \quad (8)$$

The above reaction takes place at the entire TiO_2 / redox electrolyte solution interface. In **Fig. 5**, a graph plotted V_{oc} *vs.* ℓn $[I_3^-]$ shows the dependence of open-circuit voltage on recombination reaction.

2.5 Electron transport in Mesoporous Semiconductor Oxide

The mesoporous semiconductor film is formed by interconnecting numerous nanocrystals. The main driving force for electron transport in mesoporous TiO_2 has been attributed to the gradient in electron concentration and electronic transport occurs by diffusion.[23-25] The diffusion process is coupled with ions from electrolyte through a weak electric field. This is described by an ambipolar diffusion model. [26, 27]

$$D_{amp} = n+p/(n/D_p) + (p/D_n) \quad (9)$$

D_{amb} is the ambipolar diffusion coefficient and negative and positive charge carrier concentrations are represented by n and p, respectively. The D_n and D_p are, respectively, the diffusion concentrations of negative and positive charge

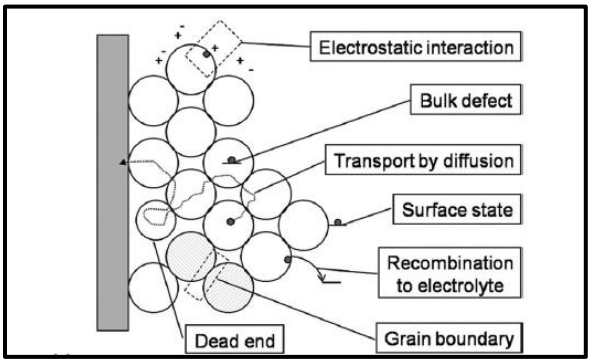

Fig.6 Overview of Electron diffusion in DSC. Traps can be located at TiO_2/electrolyte interface, grain boundaries or in bulk of TiO_2.[6]

carriers. It is also observed that electron transport depends on the incident light intensity, *ie*, the higher the intensity the faster the transport.[28,29] At lower intensities, there are chances for the electrons to get trapped in the localized states below the conduction band. The different traps located at TiO_2/electrolyte interface, grain boundaries or in bulk of TiO_2 have been depicted in **Fig. 6**.

2.6 Reactions at Counter Electrode

Transport of redox mediator in the electrolyte is driven by a diffusion process. This leads to diffusion impedance which acts as series resistance in the solar cell. The diffusion impedance depends on the diffusion coefficient, concentration of redox mediator and the distance between two electrodes. [30] Triiodide is reduced to iodide at the counter electrode of DSCs.

$$I_3^- + 2e^- \rightarrow 3I^- \quad (10)$$

Pt coated on the counter electrode acts as catalyst for the above reaction. It ensures rapid reaction and low overpotential at the counter electrode.

The alternatives to I^-/I_3^- have been widely investigated and proved successful in DSCs. The good solubility and redox properties of transition metal mediators of ferrocene/ferrocenium,[31] copper(I)/(II) complexes,[32] Ni(III)/Ni(IV) bis(dicarbollide)[33] make them a good alternatives for conventional redox shuttles. The Co-polypyridyl complexes have more positive redox potentials which should contribute higher V_{oc} in DSCs; however these are limited by slow mass transport and quick recombination between electrons and Co redox compared with the iodide [34-36].

3. Theoretical framework of Light Scattering

Scattering of light may be described as redirection of electromagnetic (EM) waves when it encounters an obstacle. When the EM waves interact with particles, electronic orbitals of molecules would be perturbed periodically with the same frequency as the incident light waves. The oscillation of electron cloud induces a dipole moment to the molecule. This oscillating dipole moment is a source of EM radiation, which results in the scattering of light. In elastic scattering, the scattered light (by particles) has same frequency as incident light wave. The light scattering theory is mainly categorized into two theoretical frameworks. One is the Rayleigh scattering theory applicable to small dielectric (non-absorbing), spherical particles. Another one is proposed by German Physicist Gustav Mie, known as the Mie scattering theory which is applicable to most spherical scattering systems. Mie theory has no particle size limitations; it is applicable to even large particles. So the Rayleigh theory is just a special case of Mie theory. The Rayleigh scattering is limited by the condition that $\alpha << 1$ and $|m|\alpha << 1$ where $\alpha = 2\pi a/\lambda$, where a is the spherical particle radius and λ is the relative scattering wavelength defined as

$$\lambda = \lambda_o / m, \quad (11)$$

where λ_o is incident wavelength with respect to vacuum and m_o is the refractive index of medium. Refractive index of scatterer (m) defined as

$$m = n - i\kappa \quad (12)$$

where n represents the refraction of light and complex part is related to absorption. Absorption coefficient is related to the complex term in the above equation by:

$$\text{Absorption coefficient} = 4\pi\kappa/\lambda \quad (13)$$

The Rayleigh scattering is only applicable to particles which are having dimensions much smaller than incident wavelength. Intensity of Rayleigh scattered light by single particle can be calculated

$$I = I_0 \frac{1+\cos\theta}{2d^2} \left(\frac{2\pi}{\lambda}\right)^4 \left(\frac{m^2-1}{m^2+2}\right) r^2 \quad (14)$$

Where I_o is intensity of incident light, d is distance to the particle and θ is the scattering angle. Rayleigh scattering cross section σ is given by the equation,

$$\sigma_{scat} = \frac{2\pi^5}{3}\frac{2r^2}{\lambda^4}\left(\frac{m^2-1}{m^2+2}\right)^2 \quad (15)$$

Mie theory is applied to explain scattering from spherical particles regardless of whether the material is light absorbing or non-absorbing. Mie scattering efficiency is determined by the equation [37]

$$Q_{scat,\,Mie} = \frac{\sigma scat,Mie}{\pi r^2} \quad (16)$$

CREATED USING THE RSC ARTICLE TEMPLATE (VER. 3.0) - SEE WWW.RSC.ORG/ELECTRONICFILES FOR DETAILS

ARTICLE TYPE

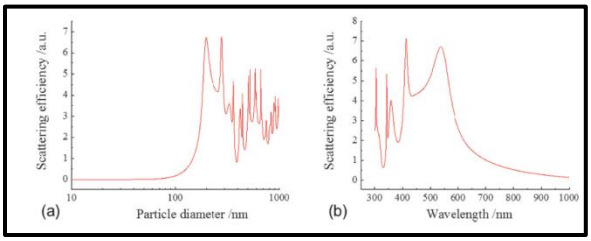

Fig.7 Shows the dependence of scattering efficiency on a) particle diameter and b) incident wavelength.[37]

where $\sigma_{scat,\ Mie}$ is the cross-section of Mie scattering given by

$$\sigma_{scat,\ Mie} = \sum_{n=0}^{\infty} 2n+1\ (\ a_n\ ^2 + b_n\ ^2 \qquad (15)$$

Where a_n and b_n are stated by the Riccati Bessel functions ψ and ζ. **Fig. 7** illustrates the dependence of scattering efficiency on the incident wavelength and the particle size. The particles having size comparable to the incident wavelength will scatter effectively. In **Fig. 7a**, the incident wavelength ($\lambda_{incident}$) is set to 532 nm, so the effective scattering is produced by particles having sizes above 200 nm. **Fig. 7b** shows that particles with 200 nm size scatters incident light in the region 400-550 nm wavelengths.

4. Survey on Materials for Light Scattering in DSCs

Colloidal science tells us about preparation of very small semiconductor particles and how to stabilize these aggregates with respect to coagulation. Colloidal particles normally have sizes less than 1000 Å. Particles show quantum effects when they become smaller than the 'first exciton Bohr radius'. Optical properties can be changed considerably in this size domain. Nanometer sized particles arranged to thin films provide enormous inner surface area. [38,39] Semiconductors absorbs light below a particular wavelength λ called the fundamental absorption edge. [40]

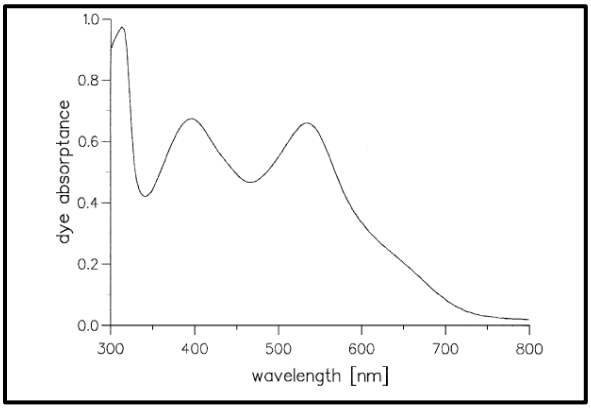

Fig.8 Spectral response of Ru Dye in DSSC.[48]

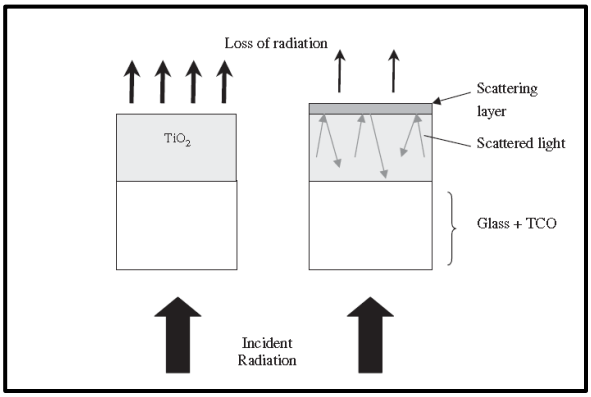

Fig.9 A model showing enhancement of scattering in DSC after introducing scattering layer.[65]

$$\lambda\ (\text{nm}) = 1240/E_g\ (\text{eV}) \qquad (17)$$

Extinction of light has an exponential dependence given by:

$$I = I_0 \exp(-\alpha \ell) \qquad (18)$$

where ℓ is the penetration length of the light and α is the reciprocal absorption length. Due to quantum effects, band edge absorption is influenced by particle sizes. TiO_2 is a widely used material in nanotechnology-assisted applications such as solar cells. In DSCs, TiO_2 film on conductive glass substrate (FTO) acts as the photoanode. Conductivity of the TiO_2 film is increased under UV illumination whereas it is very low in the dark at room temperature.[41-44] When the semiconductor is immersed into the electrolyte, the electrolyte is distributed such as semiconductor/electrolyte junction is formed at each nanocrystal. During illumination, electron-hole pair is formed and the hole-transfer to the electrolyte must be faster than the recombination of electrons. An electrochemical gradient is created by this process. Electron is transported through interconnected particles to the back contact. Charge carriers are transported *via* diffusion in the semiconductor films.

It should be noted that recombination probability is increased with increase in film thickness as electrons have to be travelled through increased number of nanoparticles and grain boundaries. [45-47] In addition; resistance loss is another loss mechanism as thickness of film is increased. So film thickness should be as thin as possible for high performance of DSC. Akira Usami proposed a theoretical concept of scattering layer of TiO_2 to improve the optical absorption of the films. [46] It is advisable to add larger particles to scatter light and improve the optical absorption. Nanoporous TiO_2 coated with dye monolayer shows poor absorption in wavelength range λ = 600-800 nm (**Fig. 8**). Optical path length of incident light can be increased by adding large particles as scattering layer. Adding too many large particles will also reduce the internal surface area of

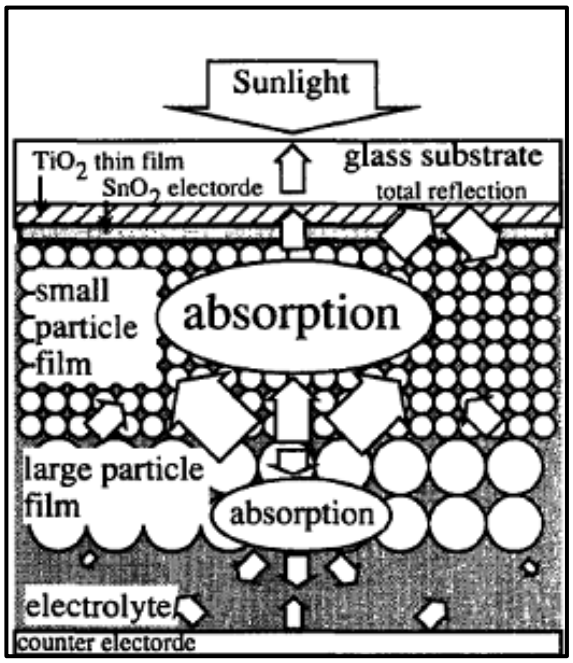

Fig.10 A newly proposed solar cell model.[46]

the TiO_2 film. The optimum thickness for the TiO_2 film is about 10-15 μm. It is obvious that as the film thickness is increased, the path length of the electrons and the redox species in the electrolyte become longer. It increases the series resistance of the film. In DSC, the working electrode normally consists of ~ 12-20 nm sized TiO_2 particles which remain transparent under visible light and eventually enhances the travelling distance of the incident light within the photoelectrode film (**Fig. 9)**.

4.1 Early studies and theoretical foundations

Barbè et al. have extensively studied the influence of processing parameters on the film microstructure at the photoanode.[47] The electrodes prepared by them using colloids autoclaved at ≤ 230 ℃ were fully transparent. Particle-size analysis was performed with different autoclaving temperatures.

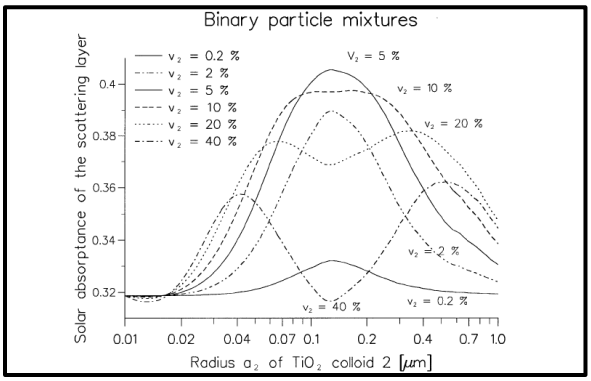

Fig. 11 The Calculated solar absorbance as function of radius of large particles.[48]

The electrodes prepared at 250 ℃ were opaque due to scattering of light by particle aggregates formed in the film. The scattering of light made a significant improvement in the photovoltaic response of the cell. The scattering of light increases the path length of photons which eventually increases its probability to interact with dye molecules. For light scattering, commercial anatase TiO_2 powder was mixed with the colloidal solution. Theoretical study on multiple scattering in DSC was carried out by Akira Usami.[46] He studied the scattering by Monte Carlo simulation method and found out scattering condition as $kd/\pi = 1.3$, where d is diameter of the particle and k is the wave number.

A new structure of DSC was proposed by Akira Usami including the idea of scattering within the solar cell (**Fig. 10**). The optimal diameter of TiO_2 particles was obtained as $1.3\sim1.4 \times \pi/k$. Computer simulations by Ferber et al. gave a clearer picture about the particle size needed to effectively scatter the sunlight in DSC.[48] The numerical solutions of radiative transport equation were used to solve multiple scattering between the TiO_2 particles.[49,50] The TiO_2 layer was assumed to be formed by mixing 20 nm particles with different fractions of larger particles. An optimal mixture was found to be 5% particles with radius 125-150 nm (**Fig. 11**). Computer simulations have shown that the fraction of large particles encourage the reflection instead of absorption and the photon absorption in near-infrared region (λ = 550-750 nm) have significantly improved. Ferber et al. further simulated a double layer structure in which back-surface scattering layer acts as a mirror. However, the effort to put a "mirror" layer was downplayed considering the small gain and enormous extra effort in cell fabrication. Rothenberger et al. have done theoretical modeling on the optical characterization of DSCs. [51] They had suggested that incorporation of large particles or voids could enhance the scattering and absorption in DSCs. Two samples were prepared for optical studies of scattering layer in DSC.

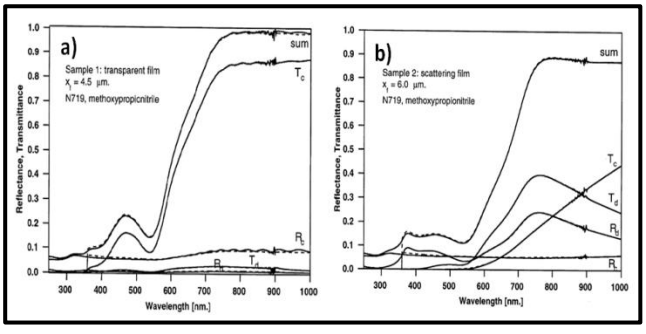

Fig.12 Transmittance and reflectance spectra for **(a)** sample 1 and **(b)** sample 2. T_c, T_d, R_c and R_s are the collimated transmittance, diffused transmittance, collimated reflectance and diffused reflectance respectively.[51]

Table 1. Different TiO_2 films with varying particle sizes.

Type of TiO_2	Porosity	Roughness factor (10μm thickness)	Average diameter (nm)
S1(synthesized in acidic solution)	0.66	1450	14.0
S2(synthesized in acidic and basic solutions)	0.59	1090	22.3
S3 (commercial)	0.61	630	37.5

Sample 1 consisted of a 4 μm thick film of anatase TiO_2 with diameter of about 15 nm and sample 2 of 6.0 μm thick films of anatase particles with diameter of about 150 nm.
The specific surface area (BET) is reduced to 35 m^2/g (sample 2) from 101 m^2/g (sample 1) as the size of the particle is increased. In **Fig. 12**, sample 2 shows a low diffused transmittance. As the particle size was increased, the sample 2 has shown a decrease in T_c and increase in T_d and R_d. The major share of collinear reflectance is from the interface of substrate glass. So there is a great potential in anti-reflecting materials that can be used in substrate glass to improve solar cell efficiency. In the solar cells, the absorption of light is limited by backscattering and diffused reflection. Tachibana et al. had indirectly studied relation between the optical thickness and the electron-transfer yield in DSCs. [52]

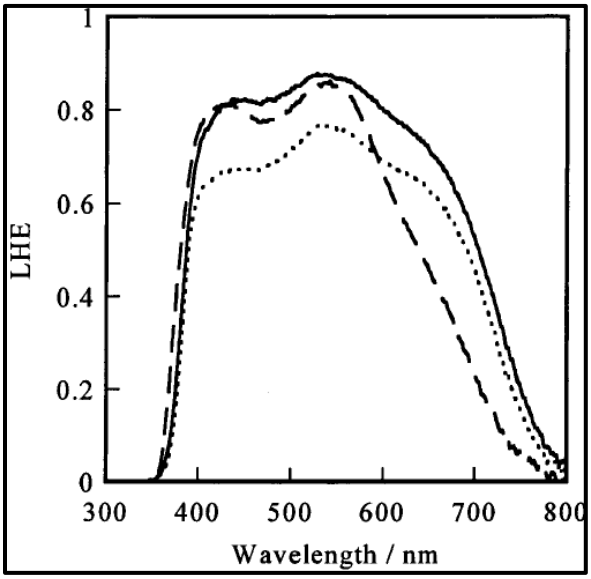

Fig.13 Harvesting Spectra for S1 (broken line), S2 (solid line) and S3 (dotted line).[52]

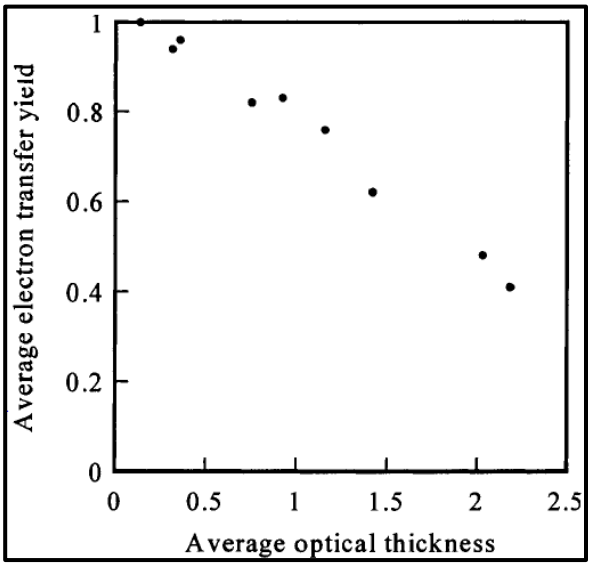

Fig.14 Relation between average electron-transfer yield and average optical thickness.[52]

The photocurrent in solar cell, determined by both LHE and electron-transfer yield is given by:

$$J_{sc} = \Phi_{ET} \int qF(\lambda)\,[1 - r(\lambda)]\,LHE(\lambda)\,d\lambda \qquad (19)$$

where Φ_{ET} is average electron-transfer yield term, q is the electron charge, $F(\lambda)$ is the incident photon flux density at wavelength λ and $r(\lambda)$ is the incident light loss
Tachibana et al. used differently sized TiO_2 particles and absorption of photons was observed by using UV-Vis steady-state absorption spectrometer. Light scattering was featured by monitoring transmittance and reflectance of unsensitized TiO_2 film. Light harvesting efficiency was also obtained with same configuration of particles which are sensitized by the ruthenium-based dye. The absorption ratio was calculated by comparing both sensitized and unsensitized TiO_2. Then the value was corrected for incident light loss at the glass substrate because the absorption and reflection by conducting glass would affect the LHE of sensitized TiO_2. Different films used by them are given in **Table 1**. In **Fig 13**, absorption spectra of different films have been depicted. The film S1 was a transparent film, which shows the characteristic absorption spectra of dye itself. Optical path has been increased by the addition of large particle into the film. So the absorption at the wavelength greater than 600 nm has been increased (i.e. Film S2). There was lowering of LHE when excessive large particles (i.e. Film S3) were added to the film. It should be noted that average electron-transfer yield was decreased with increasing average optical thickness (as shown in **Fig. 14**). In extremely light scattered condition, dye excitation becomes inhomogeneous which in turn reduce the electron-transfer yield.

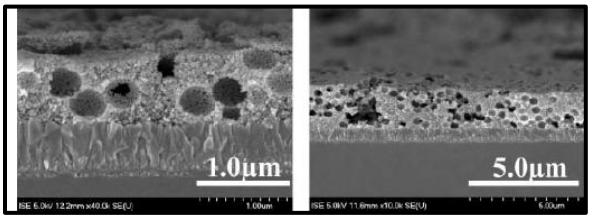

Fig.15 Spherical voids in the TiO_2 film.[53]

4.2 Different Nanostructures as light scatterers

4.2.1 Spherical voids as light scatterers

Hore et al. incorporated spherical voids as scattering centers in TiO_2 thin film.[53] Carboxyl stabilized polystyrene spheres had been used to make spherical voids since carboxyl groups are known for anchoring onto the TiO_2 surfaces. [54, 55] Polystyrene spheres were added to the TiO_2 paste in a volume ratio 1:5 and thoroughly mixed by ultrasonic bath at room temperature. Upon sintering at 450 ℃, polystyrene spheres had melted leaving voids in the film (**Fig. 15**). Mie theory was used to calculate scattering from spherical voids filled with the electrolyte.[56] Scattering cross-section (σ_s) per volume is an estimate of scattering effectiveness per volume fraction. The absorption was enhanced within the film when scattering angle was very large. It is evident from **Fig. 16** that spherical voids of about 50-100 nm could act as very good backscatterers. It was shown by using electrochemical impedance spectroscopy that the spherical voids facilitate the diffusion of ions. By the introduction of spherical voids in the TiO_2 film, the overall efficiency of device was improved by 25%.

Carbon spheres could also be employed to make pores in the TiO_2 film.[57] Yang et al. fabricated carbon spheres of different sizes (250, 500 and 700 nm, respectively) by hydrothermal method to study the influence on LHE and hence the performance of DSCs. Carbon spheres were mixed with TiO_2 slurries with different concentrations and different photoelectrodes were fabricated.

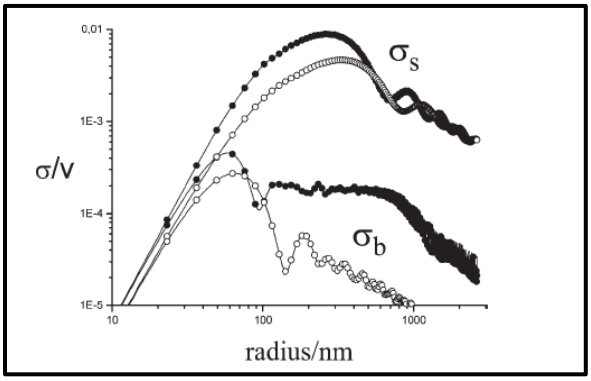

Fig.16 Total (σ_s/v) and backward (σ_b/v) scattering coefficient per volume as function of particle radius (white dot indicates presence of electrolyte filled voids in the film and Black dot, presence of solid particles in the film.[53]

It was heated at 450 ℃ for 2h to remove carbon spheres completely. The optimal concentration of carbon spheres were found to be 15 wt.% to the mass of TiO_2 nanocrystalline contained in the slurry. The best solar cell performance given by photoanode with carbon spheres of 500 nm size in TiO_2 film was 7.2 %.

4.2.2 Nano-composites for Light Scattering

Nanowire-nanoparticle composite

One-dimensional (1D) structures like nanowires can enhance light scattering and electron transport. Nanowire/nanoparticle composite has shown notable improvement in solar cell efficiency. The light scattering is considerably improved by the incorporation of nanowire with lengths in the range of hundreds of nanometers to micrometers which would provide the same effect as inclusion of large nanoparticles in the film (typically with a diameter of 100 nm). Mixing 5 wt. % of nanowires in nanoparticles shown an overall solar efficiency improvement from 5.84% to 6.24%.[58] Improvement in the light harvesting efficiency was reported by Baxter et al. by depositing ZnO nanoparticles in interstitial voids between ZnO nanowires.[59] Tan et al. extensively studied solar cell performance using nanowire/nanoparticle composites at the photoanode.[60] DSC performance was studied for different wt.% of hydrothermally grown TiO_2 nanowires in TiO_2 nanoparticles in which cell with 20 wt.% nanowires has shown an efficiency of 8.6%. The photoanodes became opaque with 77 wt. % nanowire concentration. The current density was lowered at higher concentrations of nanowires.

The DSCs showed higher open circuit voltage and fill factor because of reduced recombination and low internal resistance inside the nanowire/nanoparticle composite film. So an optimal concentration of nanowire in the film would provide critical improvement on the solar cell performance.

Nanofiber-nanoparticle composite

A composite of electrospun TiO_2 nanofibers and TiO_2 nanoparticles deposited on the photoanode has shown an improvement in light harvesting without much compromise on dye adsorption capability. [61]

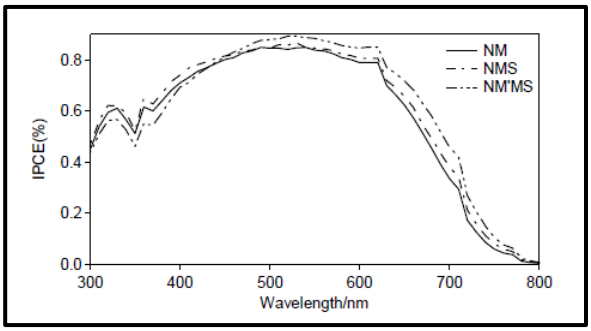

Fig.17 IPCE (%) as function of Wavelength for double layer and multi-layer photoanode.[64]

CREATED USING THE RSC ARTICLE TEMPLATE (VER. 3.0) - SEE WWW.RSC.ORG/ELECTRONICFILES FOR DETAILS

ARTICLE TYPE www.rs

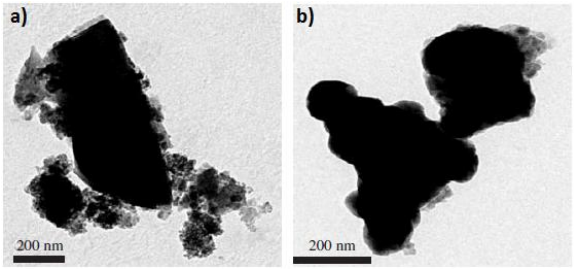

Fig.18 TEM image of rutile TiO_2 with small TiO_2 and b) ZrO_2.[65]

The cell efficiency was improved by 44% by using nanofiber-nanowire composite than using TiO_2 nanoparticles alone.

The intensity of scattered light (I) by nanofibers is calculated by following equation [62]

$$I = \frac{Io}{r}\pi\ m-1\ ^2\quad \frac{a^2}{\lambda}\quad \frac{J1\ \frac{4\pi a}{\lambda}\ \sin\frac{\theta}{2}}{\sin\frac{\theta}{2}}\ ^2 \qquad (20)$$

Where I_o is the incident light intensity and λ is the wavelength. Here r is the distance from nanofiber to the point under study, 'm' and 'a' are refractive index and radius of nanofiber respectively. J_1 is the Bessel function and θ is the angle between directions of r and incident light. From the above equation, the intensity of light scattering is to be increased substantially when nanofiber diameter is about 200 nm or above.

For the TiO_2 nanofiber-nanoparticle composite, electrospun nanofibers [63] were dispersed in anhydrous ethanol followed by adding the nanoparticle paste. Then the mixtures (with different nanofiber/nanoparticle ratios) were sonicated for uniform distribution of nanofibers and heated at 450 ℃ for 1 h to obtain the composites.

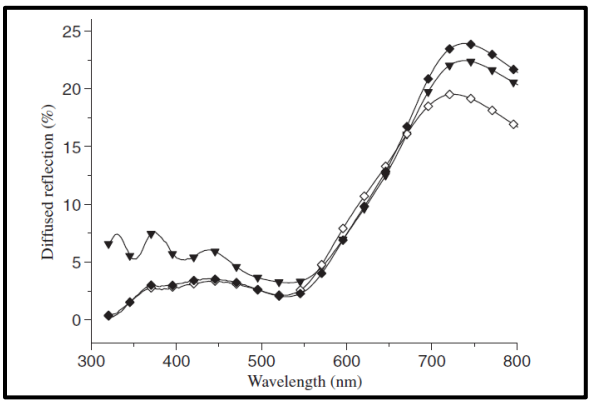

Fig.19 Diffused reflection of different scattering layers on TiO_2 film in a complete device. Scattering layers are mixtures of TiO_2-Rutile and ZrO_2 in the following propotions.25:75 (♦), 50:50 (▼) and 75:25 (◊).[65]

The electrospun TiO_2 nanofibers had diameters of about 200 to 300 nm and tens of microns length.

Randomly distributed nanofibers would scatter the light effectively to enhance light harvesting. The forward scattering was increased with increasing the diameter of the nanofibers. Dye-sensitized composite with 15% nanofibers showed a lesser transmission of light which implies a higher amount of light scattering. It has been suggested that 7.5μm thick film of 15% nanofiber is ideal for high efficiency DSC which has shown an energy conversion efficiency and short circuit current density (J_{sc}) of about 8.8% and 16.8 mA cm^{-2} respectively.

4.3 Light scattering layer using Nanostructures - A Double layer approach in DSCs

Wang et al. fabricated different types of photoanodes (monolayer, double layer and multilayer) using TiO_2 nanoparticles with various sizes of 23 nm, 50 nm and 100 nm, respectively. [64] In the monolayer configuration, when large particles of 100 nm were incorporated in the film, an improvement in IPCE (%) was observed due to the light scattering effect and the overall efficiency increased from 7.6% to 8.4%. A double layer structure had also been tried because large particles near the conducting glass in monolayer will cause backscattering. A separate layer for light scattering will reduce the backscattering loss. There was an overall efficiency enhancement from 8.4 to 9.2%. The multilayer film structure had shown an improved IPCE (%) compared to the monolayer and double layer photoelectrodes. (**Fig. 17**)

4.3.1 Large particles

The inclusion of scattering layer made up of large particles above the high surface area TiO_2 film could enhance current density by 80%. Hore et al. tried rutile TiO_2 and zirconium dioxide (ZrO_2) as scattering layers in varying proportions. [65] The light scattering depends upon change in the refractive index between the active and scattering layers. A mixture of ZrO_2 (with refractive index of 2.1), and rutile TiO_2 (refractive index of 2.8) has also been applied as scattering layer. The scattering layer was prepared from commercially available powders of ZrO_2 and rutile TiO_2 with particle sizes about 500-1000 nm. The **Fig. 18** shows TEM image of rutile TiO_2 and ZrO_2. These powders were dispersed in a 10% ethyl cellulose and α-terpineol solution. Mainly four types of scattering layers were applied on nanocrystalline TiO_2 film such as rutile TiO_2, mixture of rutile TiO_2: ZrO_2 (25:75), mixture of rutile TiO_2: ZrO_2 (50:50) and ZrO_2 alone. Reflectance and transmittance were measured for the sandwiched configurations. DSC with mixture of rutile TiO_2: ZrO_2 (25:75) as a scattering layer has shown a higher current density amongst all the cells (**Table 2**). As shown in **Fig. 19**, the diffused reflectance is maximal for rutile TiO_2:ZrO_2 mixture.

Lee et al. prepared two types of TiO_2 pastes of sizes 20 nm and 123 nm, respectively, by sol-gel method.[66]

Table 2. Current densities shown by different cells with different scattering layers.[65]

DSSC	Current Density
Without scattering layer	7.6
TiO_2	11.88
TiO_2:ZrO_2(25:75)	14.2
TiO_2:ZrO_2(50:50)	14.16
ZrO_2	12.72

A dense layer of 9 nm particles was deposited on the FTO glass substrate. Large particles (*i.e*, 20 nm and 123 nm) were used as scattering layer in DSC. Lee et al. observed a lesser transparency for multi-layered TiO_2 film with the scattering layer than the mono-layered TiO_2 films. An efficiency of 6.03% was achieved with PEG electrolyte-based DSC when 123 nm sized TiO_2 was used as light-scattering layer. Chou et al. tried TiO_2 with different particle sizes for light-scattering layer varying from 99.8 to 460.9 nm. [67] The short-circuit current density increased from 16.16 mA/cm^2 to 16.71 mA/cm^2. Cauliflower-like TiO_2 rough spheres synthesized by hydrolysis of Ti $(OBu)_4$ by using tri-block copolymer as the template was used to make photoelectrode and it has shown an efficiency up to 7.36%, which is higher than that from smooth ones. [68]

Chiba et al. have investigated the dependence of haze factor of TiO_2 photoelectrode on power conversion efficiency of the DSCs.[7] Haze factor is defined as the ratio of diffused transmittance to the total transmittance. The light scattering by TiO_2 electrode depends not only on the particle size of TiO_2 but also on preparation methods (like casting methods, sintering temperature) and atmosphere.

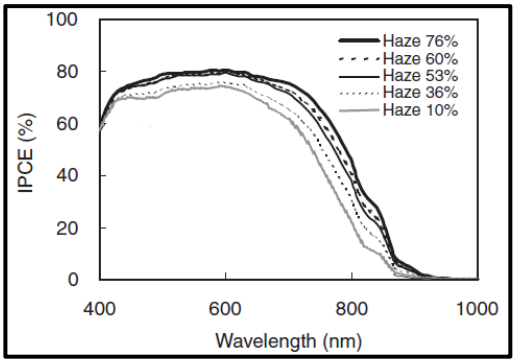

Fig.20 Dependence of IPCE (%) on the haze of TiO_2 film. (Adapted from *Jpn. J. Appl. Phys.*, 2006, **45**, L638.)[7]

So the haze is considered as the index of light scattering for obtaining better power conversion efficiencies and reproducibility. The haze was controlled by addition of sub-micron TiO_2 particles (~ 400 nm) to the electrodes. **Fig. 20** shows the dependence of IPCE (%) on haze. The high IPCE at infrared region demands high haze TiO_2 where the extinction coefficient of dye is very small (200 mol^{-1} cm^{-1}) (where as in the visible region molar extinction coefficient of the commercial dyes is very high, so medium haze is only required at this region). The 76% haze in the TiO_2 electrode shows maximum IPCE at 800 nm wavelength and with this high haze factor they have achieved a record efficiency of 11.1% with highest Jsc of 21 mAcm^{-2}. It has evolved that haze of TiO_2 photoelectrode has important role in deciding the device performance.

4.3.2 TiO_2 Nanotubes

Nakayama et al. studied nanotubes (NTs) as scattering layer in DSC.[69] Nanotubes having dimensions that are not comparable with the wavelengths of incident light; do not generally scatter the light. The light scattering happens due to the presence of grain boundaries and voids among the nanotubes which are having sizes comparable to the wavelength of the incident light. Nanotubes prepared by the anodization method were dispersed in *tert*-butanol to obtain TiO_2 nanotube suspension. Light scattering layer was deposited on nanocrystalline TiO_2 by electrophoretic deposition (EPD). The overall efficiency of DSC using nanotubes as the scattering layer has significantly been improved to 7.53% from 6.91% when large particles were used as the scattering layer.

The DSCs with nanotubes film shows a higher current density as compared to nanoparticle based DSCs. This enhancement in J_{sc} is mainly due to light scattering by the nanotubes. But the conversion efficiencies of both different morphologies were obtained as more or less same. This discrepancy is attributed to lesser fill factor reported by nanotube based DSCs. The insulating oxide layer formed between the NTs and the substrate during anodization process lowers the FF of the NT DSCs. So the nanotube applied as light scattering layer in DSCs is more favorable which would avoid the possibility of formation of the insulating oxide layer at the substrate/material interface.

4.3.3 TiO_2 Nanowires

Corn like TiO_2 nanowires were used as scattering layer in DSCs which possess high surface area and light scattering capability (**Fig. 21**).[70,71] Introduction of corn like 1D nanowires in DSC contributed to a significant increase in efficiency by 12% (7.11% for corn like TiO_2 nanowires against 6.34% for regular TiO_2 nanowire cell). Corn like nanowires and regular nanowires were prepared by two hydrothermal operations. The regular nanowires were prepared as per following procedure. One gram of TiO_2 powder in 10 M aqueous NaOH chemically treated in autoclave at 180 ℃ for 48h to obtain hydrogen titanate. This was further washed with dil.HCl and dried at 25 ℃.

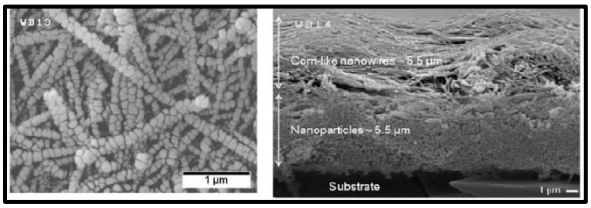

Fig.21 a) FE-SEM image of surface morphology of anatase TiO_2 corn-like nanowire, **b)** FE-SEM image of cross-sectional view of photoanode TiO_2 corn-like nanowire as scattering layer.[70]

To obtain regular nanowire, the hydrogen titanate was treated in autoclave with deionized water at 180℃ for 12h. The corn like nanowires were grown also by consecutive two hydrothermal operations as carried out to obtain regular nanowire except the process temperature and time were controlled to result hydrostatic stress for crack formation. The temperature and time for the both hydrothermal processes were set at 180℃ for 72h. The following mechanisms have been attributed as the reasons for the increase in DSC efficiency: a) corn-like TiO_2 nanowires with high surface area provided an enhanced dye sensitization due to which photon absorption is increased, and b) a lower recombination loss when corn-like nanowires were used due to their one dimensionality.

4.3.4 TiO_2 nanospindles

Qiu et al. executed a double layer structure consisting of larger anatase TiO_2 nanospindles as light scattering layer and smaller anatase TiO_2 nanospindles as underlayer for DSCs (**Fig. 22**).[72] The hydrothermal treatment of hydrogen titanate in water and different alcohols resulted in formation of the different nanospindles. The large nanospindles were obtained in water/ethanol solution whereas small nanospindles in water/ethylene glycol. In such a configuration, the small nanospindles facilitate an improved dye loading whereas large ones help in light scattering in the visible and N-IR region. In addition, recombination with I_3^- in electrolyte is also limited in nanospindles photoanode due to fewer traps in the photoanode. It has shown efficiency up to 8.3% with J_{sc} and V_{oc} of 16.4 mA cm^{-2} and 0.76 V, respectively.

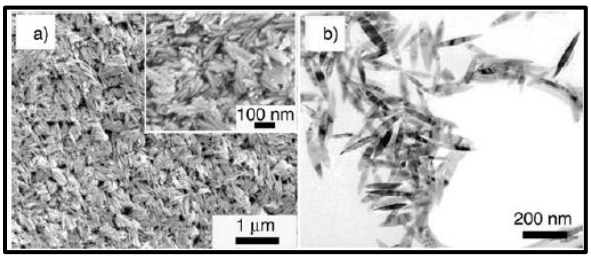

Fig.22 a) SEM **b)** TEM image of large nanospindles.[72]

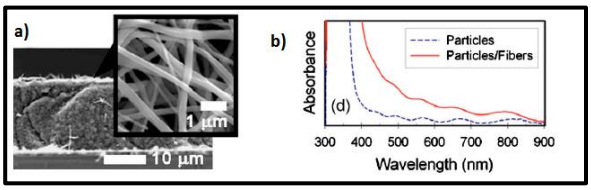

Fig.23 a) SEM image of nanoparticle/nanofiber electrode **b)** UV-visible spectra of nanoparticle film electrode and nanoparticle/nanofiber film.[73]

4.3.5 Electrospun materials

Yoshikawa et al. used 1-D TiO_2 nanofibers as scattering layer in DSCs.[73] The TiO_2 nanofibers were directly electrospun on TiO_2 paste-coated FTO (**Fig. 23a**). The solution used for electrospinning was made of 0.8g PVP, 4g of titanium (IV) butoxide and 1.175g of acetylacetone in 10 ml methanol. The nanofibers (diameter ~ 250 nm) were composed of bundle of nanofibrils (diameter ~ 20 nm). The thickness of light scattering layer deposited on nanocrystalline film was about 1 μm. An improved absorbance of light was observed for nanofibers over the nanoparticle (**Fig. 23b**). The IPCE was shot up to 85% at 540 nm when the nanofibers were used as light scattering layer which was ascribed to enhanced light scattering by TiO_2 nanofibers. An efficiency of 8.14 % was reported with a current density of 17 mA/cm^{-2} for an exposed area of 0.25 cm^2. Zhu et al. have done a comparative study by using electrospun rice- and nanofiber-shaped TiO_2, respectively, as scattering layers in DSC.[74] The active layer was made by TiO_2 commercial paste by doctor blading method on FTO. Scattering layer was fabricated by direct electrospinning of TiO_2 nanofibers on the coated working electrodes (**Fig. 23b**). The electrospinning solution was composed of 1.2g polyvinyl acetate, 10 ml N, N-dimethyl acetamide, 2 ml acetic acid and 1ml titanium (IV) isopropoxide. The average dimension for the rice grain shaped TiO_2 was about 150 nm in diameter and 400 nm in length with a high surface area of ~ 60 m^2 g^{-1}.[75,76] The fibers used as scattering layer were having an average diameter of 150 nm with a surface area of 52 m^2 g^{-1}.[77] When nanofibers were used as the scattering layer in DSC, efficiency had gone up to 7.06% against 6.44% using TiO_2 nanoparticle film alone and current density had improved from 13.6 $mAcm^{-2}$ to 14.9 $mAcm^{-2}$. With the rice-shaped TiO_2 scattering layer, the overall efficiency and short circuit current density were further improved to 7.45% and 15.7 mA cm^{-2} respectively (**Fig. 24a**). The IPCE maximum was about 74 % with the rice-shaped TiO_2 and 71% with nanofibers. The improved photovoltaic performance with the rice-shaped structures was attributed to its high surface area and single crystallinity in comparison to the TiO_2 nanofibers (less surface area and polycrystalline).

Nest-shaped TiO_2 (NS-TiO_2) nanostructures synthesized by electrospinning route is another candidate for scattering layer in DSCs. [78] The precursor solution for electrospinning was composed of 3g of PVP, 14g of titanium (IV) butoxide

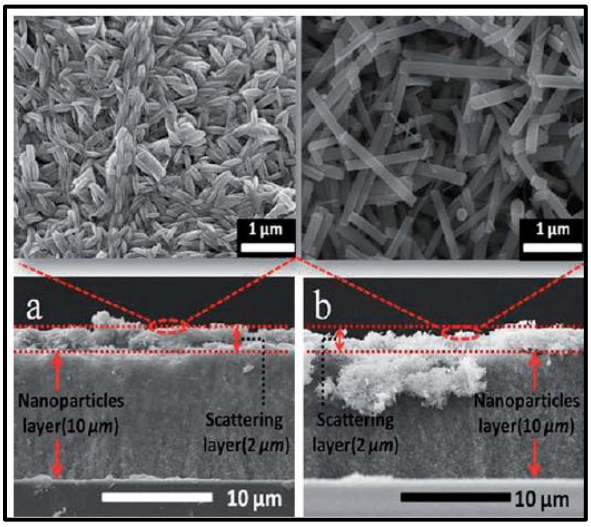

Fig.24 SEM images of Rice grain shaped TiO_2 and cross-sectional image of TiO_2 nanoparticle – Rice shaped TiO_2 nanostructure working electrode **b)** SEM images of TiO_2 nanofiber and cross-sectional image of TiO_2 nanoparticle – TiO_2 nanofiber nanostructure working electrode.[74]

and 12 mL of glacial acetic acid in 48 mL of ethanol. NS-TiO_2 nanostructures are of diameter ~ 200-500 nm with a cavity at the center (**Fig. 25a**). It was observed that the NS-TiO_2 nanostructures have a higher reflectance than P-25 which implies higher light scattering capability. The photoanode composed of 11 µm thick P25 film and 2 µm thick scattering layer on the FTO showed an efficiency of 8.02% which was about 7.1% higher compared to the ones without the scattering layer (**Fig. 25b and Fig. 25c**).

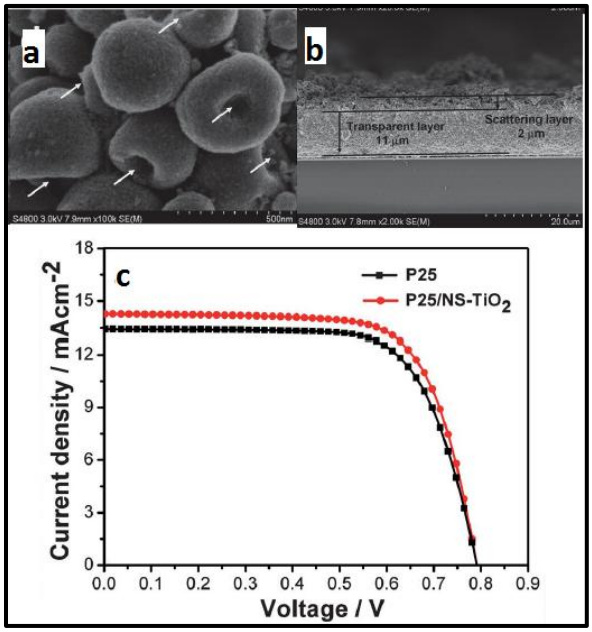

Fig.25 a) FESEM image of NS-TiO_2 nanoparticle **b)** FESEM image of P25/NS-TiO_2 electrode **c)** J-V curve of DSC with P25/NS-TiO_2 electrode.[78]

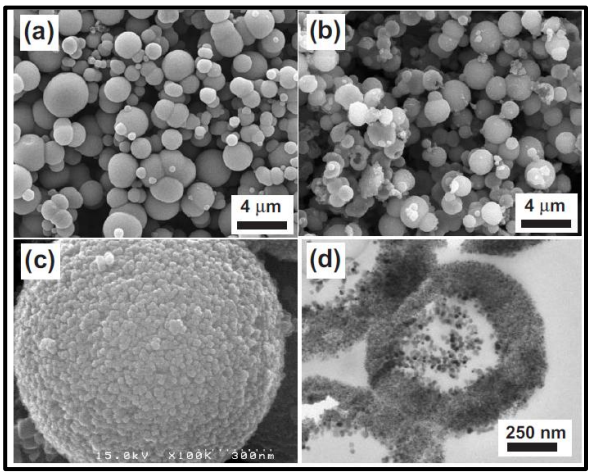

Fig.26 SEM images of **a)** synthesized NeHS TiO_2 **b)** calcined NeHS TiO_2 at 450℃ for 2h **c)** highly magnified image of calcined NeHS TiO_2 at 450℃ **d)** TEM image of a sliced NeHS TiO_2.[79]

4.3.6 Nano-embossed hollow spherical TiO_2

Nano-embossed hollow spherical TiO_2 (NeHS TiO_2) was used as bifunctional material for high-efficiency DSC.[79] The diameter of synthesized NeHS TiO_2 spheres was in the range of 1-3 µm (**Fig. 26**). The average pore size was about 10 nm and surface area obtained was 58 m^2g^{-1}.The photovoltaic characteristics of photoelectrodes, one with nanocrystalline TiO_2 film with NeHS and other with commercially available TiO_2 particles with diameter of 400 nm as the over layer were considered for the study.

The incorporation of NeHS as light-scattering over layer in the DSC resulted in an improvement of the overall efficiency from 7.79 to 9.43% (**Fig. 27**). The NeHS TiO_2 light-scattering included DSC has shown a higher photocurrent density (J_{sc}) *i.e.* 15.8 mA cm^{-1} than the other one.

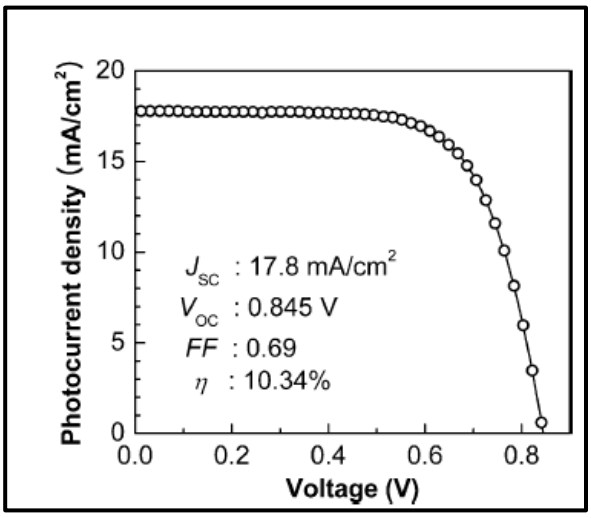

Fig.27 J-V curve of DSC based on the NeHS TiO_2 as light scattering layer.[79]

CREATED USING THE RSC ARTICLE TEMPLATE (VER. 3.0) - SEE WWW.RSC.ORG/ELECTRONICFILES FOR DETAILS

ARTICLE TYPE

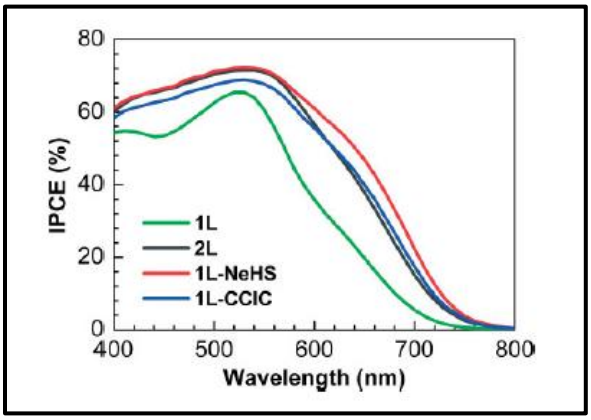

Fig.28 IPCE spectra of DSCs with 6 µm thick nanocrystalline TiO_2 film on photoanode (1L) and 12 µm thick film (2L) and light-scattering over layer of NeHS TiO_2 (1L-NeHS) and over layer of submicrometer-sized TiO_2 particles.[79]

The improvement in J_{sc} has been attributed to the enhanced dye loading capability and light scattering effect of NeHS TiO_2. The absolute IPCE was higher in the NeHS TiO_2 sample than the conventional larger TiO_2 particles (**Fig. 28**).

4.3.7 Hexagonal TiO_2 plates

The packing density is very low for microspherical particles which are conventionally used in DSCs as the scattering layer. This problem was solved by using novel hierarchical TiO_2 nanoplates with high surface area and sufficient attachment between the particles (**Fig. 29**). [80] By controlling hydrolysis and deposition process of titanium precursors, hierarchical TiO_2 was prepared by using $Cd(OH)_2$ nanoplates.[81-83] The nanoplates [84] were used as light scattering layer in a bilayer DSC model with a thickness of 4 µm and P25 as bottom layer with a thickness of 8 µm. A better reflection was obtained with increased number of mesoshells of nanoplates because of the confinement of light inside the nanoplates. The DSC fabricated with the TiO_2 nanoplates as scattering layer have shown short-circuit current density of 13.52 $mAcm^{-2}$ and an open-circuit voltage of 0.79 V. The overall conversion efficiency was about 6.53%.

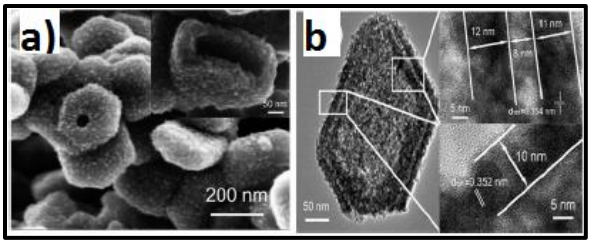

Fig.29 a) SEM **b**) HRTEM image of hexagonal TiO_2 plate.[80]

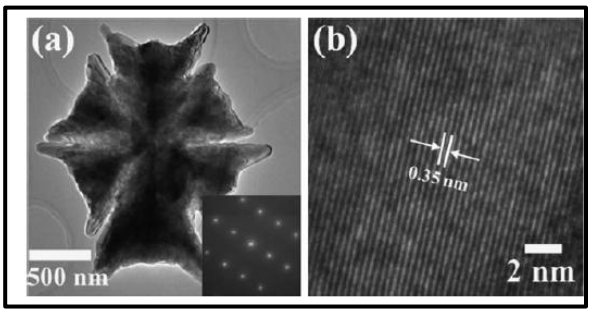

Fig.30 a) Low magnification and **b)** high resolution TEM images of a microplate. Inset of (a) is selected-area electron diffraction (SAED).[85]

The surface area of nanoplates was more or less same as P-25 and the efficiency improvement has been attributed to the enhancement of light harvesting by reflection from nanoplates. The single crystalline hexagonal TiO_2 microplates with good reflectance at the wavelength region 400-900 nm was also used as light scattering layer (**Fig. 30** and **Fig. 31**).[85] A paste of hexagonal TiO_2 was made and screen-printed over 9.5µm thick nanocrystalline TiO_2 layer on FTO glass substrate. The thickness of the scattering layer was about 4 µm. The planar structure of TiO_2 microplates helps to reflect incident light back to the nanocrystalline TiO_2. The photoanode made of nanocrystalline TiO_2 have shown an overall efficiency (η) of 6.80 % and short-circuit current density (J_{sc}) of 12.4 $mAcm^{-2}$. The introduction of commercial TiO_2 scattering layer has made an increment in the overall efficiency to 7.45%. Further superior performances were obtained with TiO_2 microplates as scattering layer with an overall efficiency of 7.91% and short-circuit current density of 14.2 $mAcm^{-2}$.

4.3.8 TiO_2 Photonic crystals

The scattering layer with larger particles in DSCs makes it opaque which will disqualify the DSCs as window panes in building integrated photovoltaics.

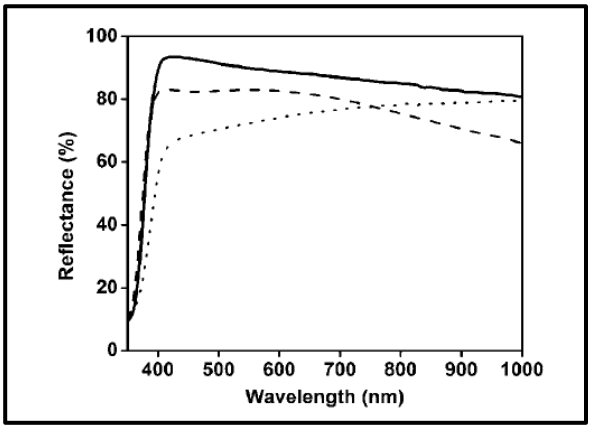

Fig.31 Reflectance spectra of TiO_2 microplate film (solid line), commercial TiO_2 scattering film (dash line), and TiO_2 microrod film (dotline).[85]

CREATED USING THE RSC ARTICLE TEMPLATE (VER. 3.0) - SEE WWW.RSC.ORG/ELECTRONICFILES FOR DETAILS

ARTICLE TYPE

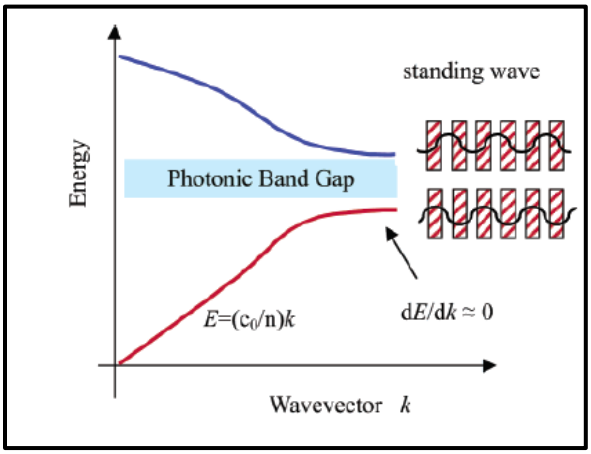

Fig.32 Optical band structure photonic crytstal.[95]

The inclusion of photonic crystals (PC) as scattering layer will help to retain transparency of DSCs to some extent. The photonic gap materials can be employed in the form of 3D inverted TiO_2 opal or porous Bragg stacks to enhance light harvesting by retaining transparency.[86-89] Different theoretical possibilities have been put forwarded for enhancing light absorption such as localization of heavy photons near the edges of photonic bandgaps,[90] Bragg diffraction in periodic lattice,[91] multiple scattering at disordered regions,[92] and via multiple resonant modes.[93] The coupling of photonic crystals in DSCs can be employed as an effective way to improve the conversion efficiency of DSCs. Light propagates in ordinary materials at (1-3) × 10^8 m/s which will take about one hundred femtoseconds to travel through 10 μm thickness. Confinement of light in the same medium reduces the velocity. Asher et al. first observed Bragg scattering with the three dimensional polystyrene colloidal crystal arrays.[94] They observed stop band in polystyrene colloids, which could be employed to reject light of specific wavelengths. Photonic crystals have three major properties which make them attractive.

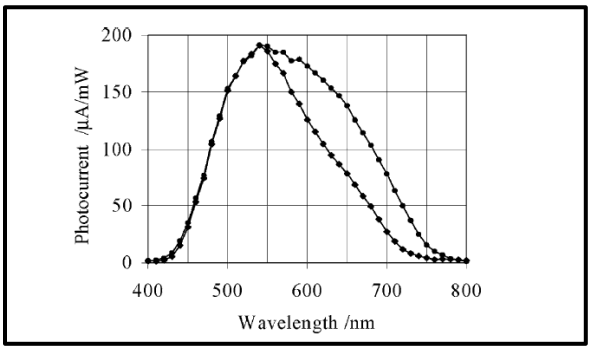

Fig.33 Wavelength dependence of the short-circuit photocurrent. Upper curve shows response of bilayer electrode and lower curve is of conventional nanocrystalline TiO_2.[95]

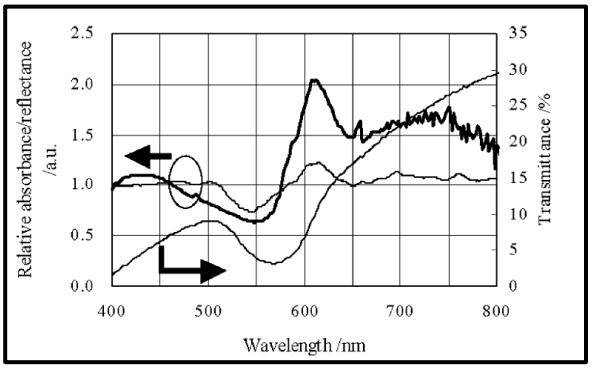

Fig.34 Relative absorption and reflectance spectral ratios. The normalized absorption spectrum of dye-sensitized photonic crystal by the dissolved dye (thick line). The reflectance spectrum of the dye adsorbed photonic crystal was normalized to that before dye absorption (thin line).[95]

- Prohibition of the propagation of particular wavelengths.
- Briefringent and anisotropic dispersion.
- Nonlinear dispersion.

Nishimura et al. studied red absorbance and photocurrent enhancement in DSCs where TiO_2 is coupled to photonic crystals.[95] Dispersion curve (E vs k) shows the group velocity of light decrement near to the wavelength of stop band [96] (see **Fig. 32**). Depending on energy, light waves would be localized in different sites of PC structure and absorber in high dielectric medium will interact more with red part of the stop band. Photocurrent response has been considerably improved at longer wavelength region over using only nanocrystalline TiO_2 film (**Fig. 33**). As in Borrmann effect in X-ray scattering, red part of the spectrum absorber will "borrow" intensity from blue part (**Fig. 34**).[97] In the study reported by Nishimura et al. TiO_2 photonic crystals (inverse opal) were coated on the FTO. Replication of colloidal crystal templates was the method adopted by them. [98-104] The suspended monodisperse carboxylate-modified polysterene latex spheres were immersed vertically in the colloidal solution which was kept at 55 ℃ for 1 to 2 days to evaporate the suspension completely. The colloidal crystal film was formed on the surface with a thickness of about 215 nm.[105] Liquid-phase deposition (LPD) method was used to infiltrate titanium dioxide into voids retaining its periodicity.[106-111] The latex spheres were removed by calcinations at 400 ℃ for 8 h, resulted in mesoporous TiO_2 with air holes. Thickness of titanium walls of the inverse opals can be controlled in second LPD to tune stop band precisely.[112] The cell was fabricated with a conventional TiO_2 coating over a 3 μm thick photonic crystal. The absorption spectra of dye-sensitized photonic crystals and the same dye in ethanol solution were compared. Absorbance was increased at red edge of the stop band of dye sensitized photonic crystals as compared to the dye in solution. A suppression of absorbance for shorter wavelength was also

CREATED USING THE RSC ARTICLE TEMPLATE (VER. 3.0) - SEE WWW.RSC.ORG/ELECTRONICFILES FOR DETAILS

ARTICLE TYPE

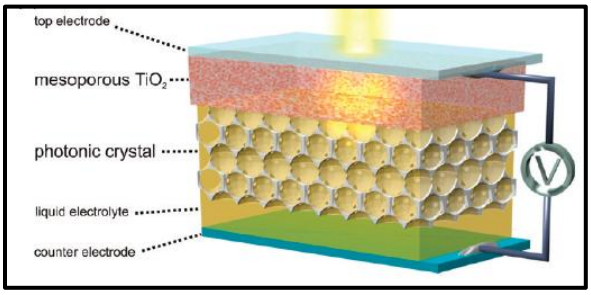

Fig.35 Shematic of 3D photonic crystals as DSCs overlayer.[114]

observed (see **Fig 34**). In this study, the bilayer electrode with nanocrystalline layer in contact with FTO was found to be unsuccessful.

Miguez et al. postulated that major part of the spectrum can only be tapped when the nanocrystalline TiO_2 is placed in between the photonic crystal and the transparent conductive oxide substrate.[113] The connectivity between the nanocrystalline TiO_2 and the photonic crystal was one of the problems in implementing photonic crystal as the over layer. Guldin et al. constructed optically active 3D photonic crystal as overlayer (**Fig. 35**).[114] Copolymer-derived mesoporous underlayer was prepared on conductive transparent substrate. The TiO_2 inverse opals was formed as the over layer with different pore sizes. To analyze the photocurrent generation, IPCE or quantum efficiency was plotted against the wavelength of both bilayered and single layered DSCs. Here for the reference, a relatively thin layer of TiO_2 with 465 nm thickness was chosen to avoid cracks on the film. A double layer DSC was fabricated with 1.4 μm thick PC overlayer on the top of 465 nm thick TiO_2 underlayer. The external quantum efficiency (IPCE) of DSCs with three different PC over layer is shown in **Fig. 36**.

The one-dimensional photonic crystals (1D PCs) are preferred over 3D PC because of their easiness in assembling a thin layer on nc TiO_2 active layer. The thick 3D PCs (5-10 microns) have adverse effect on conversion efficiency as charge transport would be limited by increased recombination in the cell.

4.3.9 Cubic CeO_2 nanoparticles

Cerium dioxide (CeO_2) cubic nanostructure with high refractive index is one of the potential candidates for enhancing light harvesting efficiency by light scattering. The mirror-like facets of CeO_2 are responsible for the scattering effect. Yu et al. have used CeO_2 nanoparticles of about 400 nm as overlayer in DSCs. [115] With a 1.5 μm thick top layer on mesoporous TiO_2, conversion efficiency has been improved to 8.6% from 7.3%. However, a reduction in dye loading was observed when CeO_2 was introduced as the top layer. [116] The diffused reflectance was very high for the bilayer photoanodes compared to pure TiO_2 nanocrystalline film. The CeO_2 overlayer enhanced the light reflectance in the wavelength region 400-800 nm (light reflectance increased over 70%). The highest current density (J_{sc}) with CeO_2 as overlayer was 19.3 $mAcm^{-2}$. The highest efficiency reported with CeO_2 as top layer was 8.6% and V_{oc} observed was about 0.69 V.

4.3.10 Surface modified particles in scattering layer

The surface of particles used as scattering layer can be modified to obtain better conversion efficiency for DSCs. Choi et al. coated Al_2O_3 on large TiO_2 particles.[117] Sol-gel method was used to modify the surface of large TiO_2 scattering particles.[118] Colloidal Al_2O_3 of various concentrations with TiO_2 powder was stirred to obtain TiO_2 suspension. The coating of Al_2O_3 on TiO_2 depends on pH of TiO_2 suspension and concentration of Al_2O_3. A few nanometer thick Al_2O_3 nanoparticles were coated over the 300-800 nm sized TiO_2 particles. The photoelectrode was made of commercial TiO_2 paste as underlayer and large Al_2O_3 coated TiO_2 as the scattering layer. The reflectance spectrum revealed that the total reflectance of TiO_2 film was considerably increased in the region 380-800 nm when a light scattering layer was introduced (**Fig. 37a**). The IPCE showed an increased photocurrent response for good oxide surface coated TiO_2 scattering layer (sample C) (**Fig. 37b**).

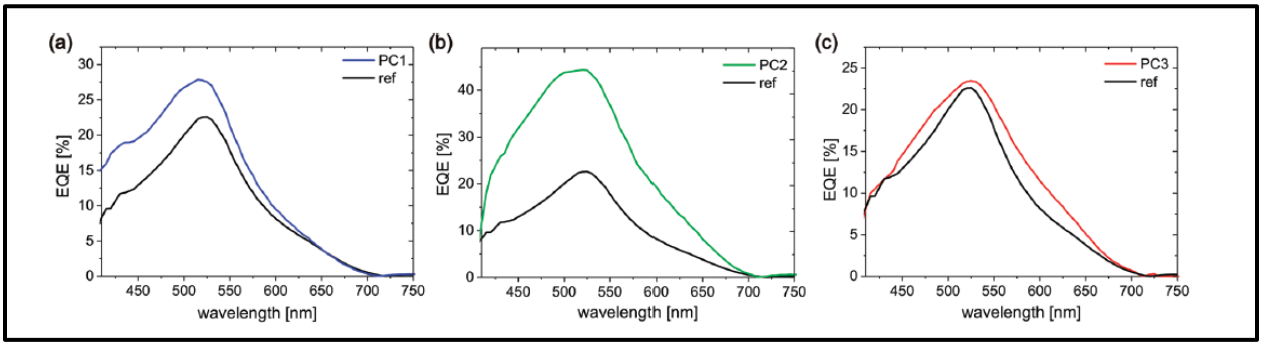

Fig.36 External Quantum Efficiency (%) of DSCs with different PC as overlayer.

PC1:3D inverse opal with diameter 240nm. (b) PC2: 3D inverse opal with diameter 260nm. (c) PC3: 3D inverse opal with diameter 350nm.[11]

CREATED USING THE RSC ARTICLE TEMPLATE (VER. 3.0) - SEE WWW.RSC.ORG/ELECTRONICFILES FOR DETAILS

ARTICLE TYPE

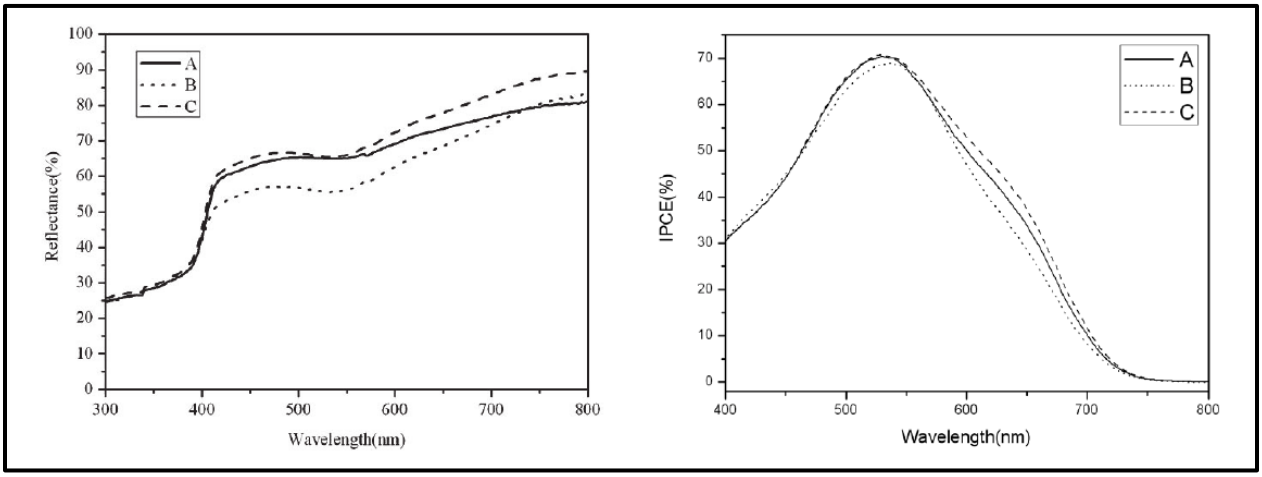

Fig.37 a) Reflectance spectrum of dye sensitized TiO_2 film of samples with light scattering layer **b)** IPCE of DSSC with light scattering layer. A: sample with a non-coated scattering layer, B: sample with TiO_2 scattering layer (with 0.235 Al_2O_2 Concentration in wt% and pH value of 12), C: sample with TiO_2 scattering layer (with 0.016 Al_2O_2 Concentration in wt% and pH value of 7).[117]

The best efficiency (8.71%) was reported for the sample C.

5. Dual function materials in DSCs

In the above sections, we examined the materials which were employed for scattering light in DSCs where the scattering material is added as an additional layer or as component. But some materials provide both higher surface area as well as light scattering capability.

5.1 Nanocrystalline spherical aggregates

Aggregates of oxide nanocrystallites would satisfy dual requirements such as high internal surface area and light scattering ability. Nanocrystallite spherical aggregates consist of spherical assembly of nano-sized oxide crystallites with submicron diameter. The nano-sized crystallites *i.e.* building blocks of aggregates provide higher internal surface area nearly equal to the nanocrystalline film. Light scattering capability is derived from the submicron size of the aggregates. Scattering by aggregates would increase travelling distance of light within the photoanode and interaction of light with the dye is enhanced. The light scattering by nanocrystalline spherical aggregates can be analytically described by the Lorentz-Mie-Debye resonance theory in which light scattering efficiency Q_{sca} given by

$$Q_{sca} = \frac{2}{x^2} \sum_{n=1}^{\infty} 2n+1 \ (an^{\,2} + bn^{\,2}) \qquad (21)$$

where x is defined as size parameter, $x = 2\pi r / \lambda$, r is the radius of sphere, λ is the incident wavelength and a_n, b_n are the complex Mie scattering coefficients. One can see that sample consisting large aggregates of diameter ~350 nm gives maximum scattering efficiency.

5.1.1 ZnO aggregates

Over the years TiO_2 has been the material of choice for DSCs. Recently, ZnO as a material alternative to TiO_2 has been widely investigated. The following reasons make ZnO a potential candidate for DSC: a) band-gap of ZnO is similar to TiO_2 (3.2eV), b) higher electron mobility of ZnO (~115-155 $cm^2V^{-1}s^{-1}$, [119] whereas that of TiO_2 is only ~10^{-5} cm^2 $V^{-1}s^{-1}$).[120] The hierarchically-structured ZnO film consisting of secondary ZnO colloids of ~ 300 nm in diameter that are made up of primary ZnO nanoparticles of ~20 nm in diameter would encourage light scattering in DSC (**Fig. 38**). The first DSC application of ZnO aggregate was introduced by Chou et al.[121] The ZnO aggregates were synthesized by hydrolysis of zinc salt in polylol medium at 160 ℃.[122,123]

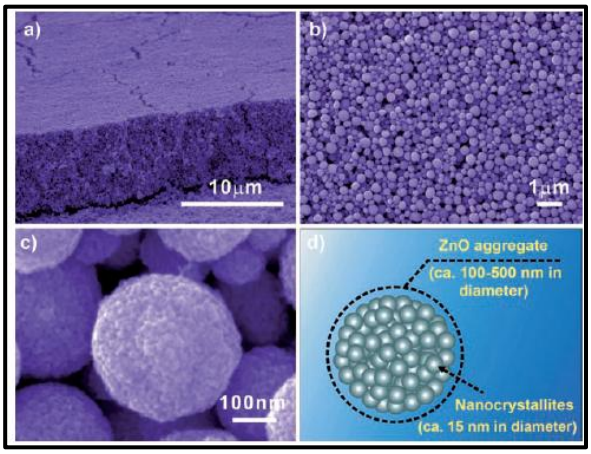

Fig.38 a) Cross sectional SEM of ZnO aggregate film **b)** SEM image of top view of polydisperse ZnO aggregate film **c)** A magnified SEM image of ZnO aggregate **d)** Schematic of ZnO aggregate comprising of closely packed nanocrystallites.[125]

CREATED USING THE RSC ARTICLE TEMPLATE (VER. 3.0) - SEE WWW.RSC.ORG/ELECTRONICFILES FOR DETAILS

ARTICLE TYPE

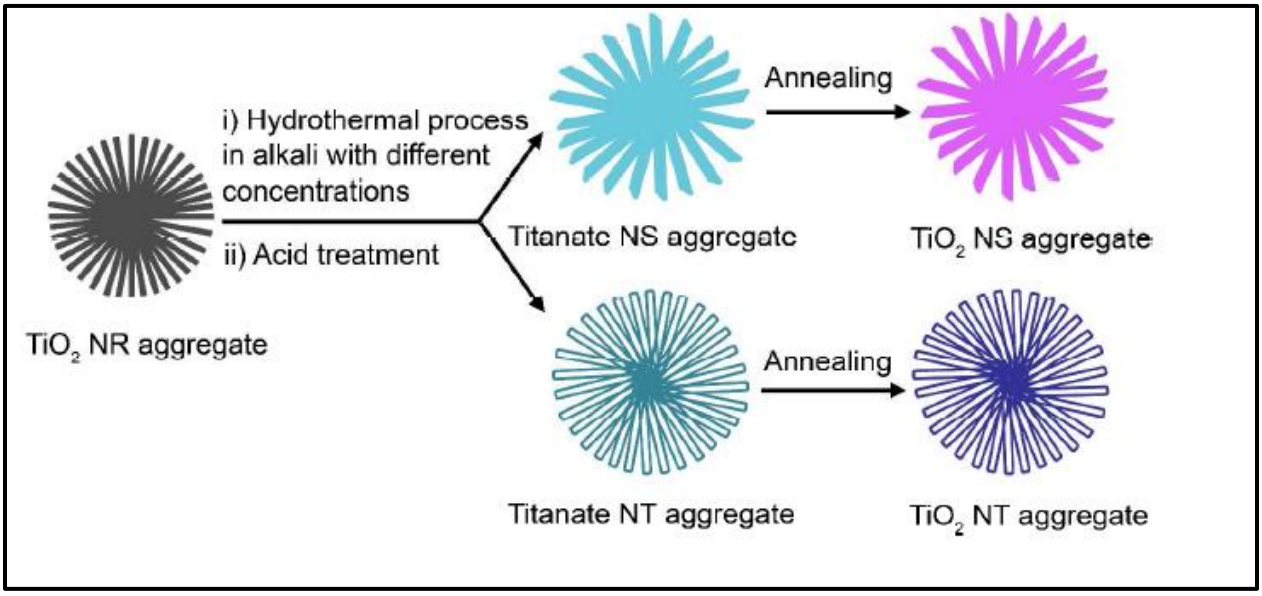

Fig.39 TiO_2 NS aggregate and NT aggregate were prepared from TiO2 NR aggregate.[134]

The aggregates were separated centrifugally from the solvent. The photoelectrode was made from suspension solution by drop casting method. [124] The specific surface area of aggregates was reported as 80 m^{-2} g^{-1} by BET measurement.[125] The large surface area provides a good dye adsorption on aggregate photoelectrode film. The optical absorbance spectrum of aggregate photoelectrode film has an additional absorption in the visible region due to light scattering, other than the intrinsic absorption of ZnO. The photocurrent peak in IPCE at 360 nm was due to direct absorption of ZnO. The sample 1 with perfect aggregates has shown highest efficiency of about 5.4%. It was found that light scattering is more intensive with aggregate size closer to incident wavelength. Memarian et al. have achieved a record efficiency of 7.5% by spray pyrolysis method. [126]

5.1.2 TiO_2 aggregates

The nanobeads or nanoporous microspheres are considered as TiO_2 aggregates. [127-130] The TiO_2 aggregates are assemblage of nanocrystallites. The TiO_2 beads are fabricated *via* hydrothermal treatment of amorphous TiO_2 beads in ammonia. The TiO_2 beads produced had a surface area of 89 m^2 g^{-1} and diameter of 830 nm. A comparison of IPCE with P25 has shown a high performance for the TiO_2 mesoporous nanobeads. A higher efficiency of about 9.1 % was reported with TiO_2 nanobeads without $TiCl_4$ treatment (after $TiCl_4$ treatment efficiency reached at 10.6%). Another advantage of TiO_2 aggregate is the higher internal surface area compared with P25 which resulted in more dye loading. It was also noted that lifetime of photoelectrons in photoelectrode film is longer than that in conventional photoelectrode film because of the close packing of nanocrystalites within the TiO_2 aggregates. Light scattering and the above mentioned uniqueness of TiO_2 aggregates contribute to the efficiency enhancement.

TiO_2 and SiO_2 aggregates synthesized by Molten Salt Method (MSM) were used in DSC applications. [131,132] The TiO_2 agglomerated nanostructures produced by MSM were of diameter ~ 100-300 nm. However, TEM studies revealed that the aggregates were actually composed of smaller nanoparticles with diameter of 5 nm. These particles were responsible for higher surface area of 200 m^2 g^{-1}. Using MSM TiO_2 a power conversion efficiency of 7.48 % was obtained. The IPCE is enhanced at small wavelength region (< 600 nm) due to high dye loading and that at longer wavelength region (> 600 nm) due to light scattering effect by aggregates of size 100-500 nm.

Tailored spherical TiO_2 aggregates

Substitution of nanorods or nanotubes as building units for the nanocrystallites in the spherical aggregates could provide excellent electron transport property without compromising on surface area and light scattering capability. Liu et al. have prepared TiO_2 nanosheet (NS) aggregates and TiO_2 nanotube (NT) aggregates from spherical nanorod (NR) aggregates.[133,134]

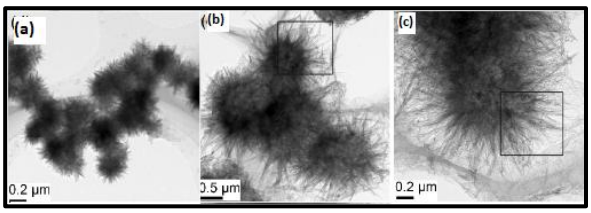

Fig.40 TEM images of a) NR aggregate b) NS aggregate c) NT aggregate.[134]

CREATED USING THE RSC ARTICLE TEMPLATE (VER. 3.0) - SEE WWW.RSC.ORG/ELECTRONICFILES FOR DETAILS

ARTICLE TYPE

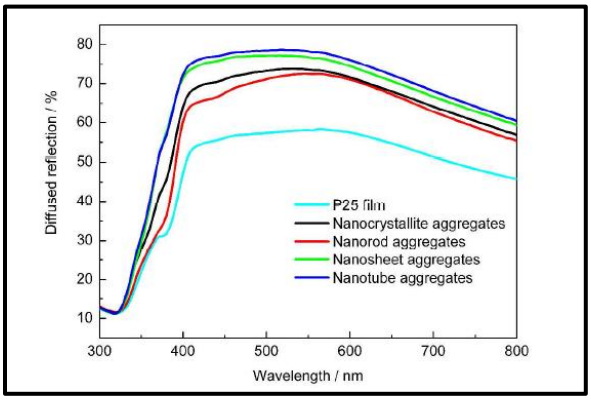

Fig.41 Diffused reflectance spectra of different tailored TiO_2 aggregate films.[134]

The TiO_2 NS aggregates were prepared by following procedure (**Fig. 39**).The TiO_2 nanorod aggregates were undergone hydrothermal treatment in 5M sodium hydroxide at 140℃ for 24h and further washing of sample by diluted hydrochloric acid. This was further annealed at 400℃ for 30 min. The TiO_2 NT aggregates were also synthesized following similar route of preparing NS aggregates except changing concentration of hydrothermal reaction solution. It is interesting that dimension of NT and NS aggregate have significantly improved from 400 nm (which is the dimension of nanorod aggregate) to 1-2μm which will ultimately increase the scattering capability of nanostructure. The TEM images have shown in **Fig. 40**. The diffused reflectance spectra have shown better light scattering property at the infrared region. A higher reflectance was obtained for the NT and NS aggregate compared to the NR aggregate (**Fig. 41**). This higher light scattering is due to the larger dimension sizes of the NT and NS aggregate. The high BET surface area have reported for NR aggregates (106.7 m^2/g), NT aggregates (134.8 m^2/g) and NS aggregates that resulted in better dye loading.

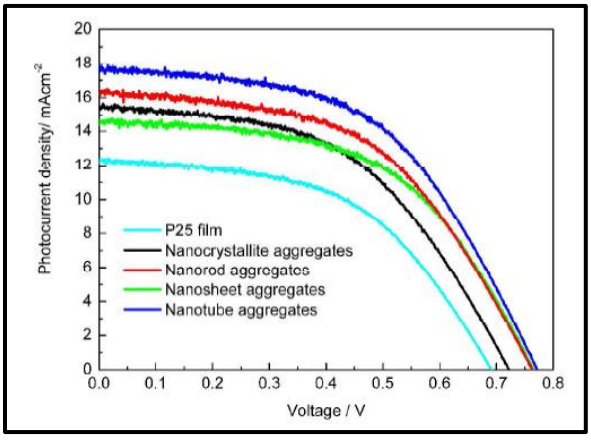

Fig.42 I-V characteristics of DSCs using different tailored TiO_2 aggregate.[134]

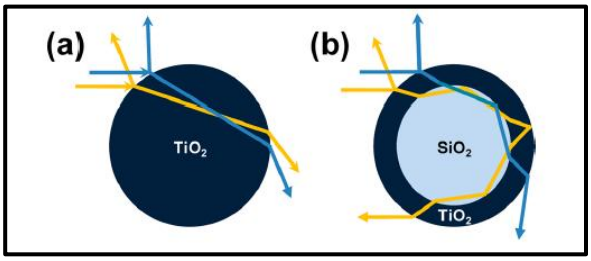

Fig.43 Schematic of light scattering by a) TiO_2 nanoparticle and b) TiO_2-SiO_2 core/shell nanoparticle.[138]

The NT aggregate DSC has reported a best efficiency of 7.48% with Jsc of 17.82 mA/cm^{-2} among this class of TiO_2 materials. The NS and NR aggregate DSC has reported an efficiency of 6.45 and 6.82 % respectively (**Fig. 42**).

6. Other innovations for light scattering in DSCs

6.1 Core-Shell materials for light scattering

Theoretical studies have been done by several research groups on the light scattering effect of core/shell nanoparticles.[135, 136] The Mie theory explains generally the light scattering by spherical particles. Arden and Kerker's scattering theory for concentric spherical particles is well suited to explain the light scattering by coated spheres (Core/shell particles). Consider a spherical, coated particle of inner radius X, outer radius Y and coated thickness Z (Y-X) which is illuminated by a monochromatic beam of wavelength λ_0. The refractive indices of the core, shell, and surrounding medium were assigned as n_1, n_2, n_0 respectively. The intensity I (θ) of scattered radiation by a single particle at an angle θ for incident radiation that is polarized perpendicularly to the scattering plane given by

$$I(\theta) = I_0 \frac{\lambda 0^2}{4(\pi r)^2} S(\theta)^2 \qquad (22)$$

Where r is the distance between the particle and point of interest, I_0 is the incident radiation and S_1 (θ) is infinite series.

$$S_1(\theta) = \sum_{n=1}^{\infty} \frac{2n+1}{n(n+1)} [a_n \pi_n(\theta) / b_n \tau_n(\theta)] \qquad (23)$$

The amplitudes a_n and b_n are functions of the size parameters x = kX and y = kY

Where $k = 2\pi/\lambda = 2\pi n_0/\lambda_0$.

High scattering efficiency was reported by Hsu et al. using core/shell nanoparticles with a diameter of 0.8-1.0 µm and shell thickness of 0.2-0.3 µm. [137] Son et al. prepared SiO_2/TiO_2 core/shell nanoparticles using SiO_2 template by sol-gel method for DSC application.[138] Monodisperse SiO_2 nanoparticles in different diameters were synthesized by

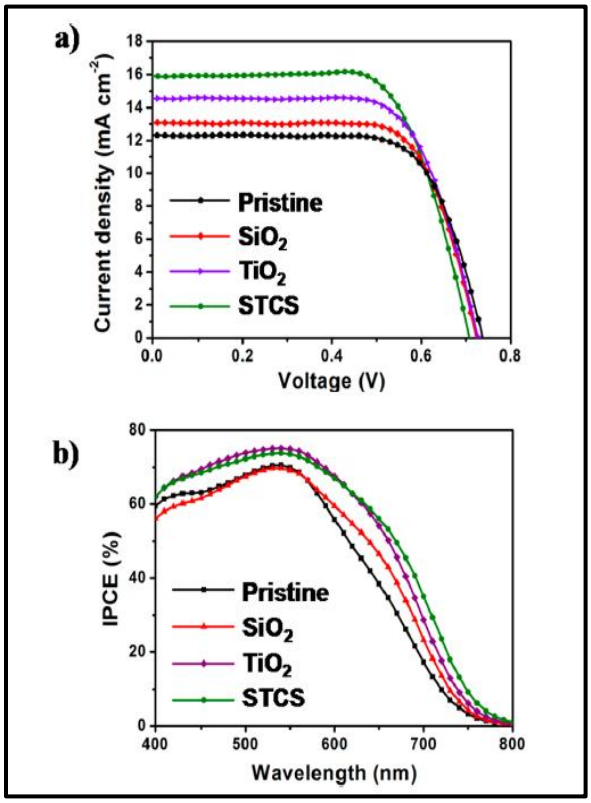

Fig.44 a) Current density – voltage curve and **b**) IPCE of DSC with SiO_2 nanoparticle,TiO_2 nanoparticle and TiO_2/SiO_2 core/shell nanoparticle as scattering layer.[138]

seed regrowth method.[139] The TiO_2 nanoparticles were coated over SiO_2 using sol-gel method. The light scattering in TiO_2 and SiO_2/TiO_2 core/shell nanoparticles was explained based on geometrical optics (**Fig. 43**)[140]. In SiO_2/TiO_2 core/shell nanoparticles, light undergoes back scattering unlike the forward scattering by larger TiO_2 nanoparticles. This will lead to optical confinement in DSCs and enhancement of the conversion efficiency. The SiO_2 nanoparticles with a diameter of 240 nm as core in SiO_2/TiO_2 core/shell nanoparticles when used as scattering layer in photoelectrode has shown a better performance compared with SiO_2 or TiO_2 as scattering layer materials. The efficiency of 7.9 % was obtained with improved current density of 15.9 mAcm^{-2} (**Fig. 44**).

6.2 Double light-scattering film

Zhao et al. fabricated DSCs with double light-scattering layer consisting of TiO_2 nanosheets as the underlayer and TiO_2 hollow spheres as the overlayer.[141] The DSC with double light scattering layer has shown superior performance compared to TiO_2 hollow sphere film alone or TiO_2 nanosheet film. An improved efficiency of 5.03 % was reported which was 23% higher than that of TiO_2 hollow sphere film alone (η=3.6%) and 8.3% higher than that of TiO_2 nanosheet film (η =4.31).

6.3 Surface Plasmon effects in DSCs

The optical properties of metal nanoparticles are influenced by collective motion of free electrons within a small sphere. [142] Electromagnetic wave induced collective motion of electrons is called as surface plasmons. The plasmonic resonance induces a dipole moment in metal nanoparticles which will eventually enhance the electric field around it and hence the optical extinctions such as absorption and scattering are also increased. Solid-state DSCs (ss-DSCs) are fabricated using hole-transport materials (HTM) replacing conventional electrolytes. It will facilitate tuning open circuit voltage by adjusting HOMO of HTM. The higher recombination [143] and incomplete hole filling of HTM [144,145] would limit thickness of active layer to 2 µm. This thickness is much less to absorb light effectively. The plasmonic effects have been employed to improve light absorption in active layers of solar cells.[146] Metal nanoparticles enhance the light absorption of solar cells both by localized surface plasmon and by light scattering. Ding et al. used nanoimprint lithography (NIL) to incorporate plasmonic back reflectors into the mesoporous TiO_2 active layer.[147] The plasmonic back reflectors were designed as 2D array of metallic domes in ss-DSCs. However the challenge before the scientific community is identifying an inexpensive route to fabricate the plasmonic structures.

The metal nanoparticles (NPs) were in direct contact with dye and the electrolyte in earlier surface plasmon assisted DSCs. It normally resulted in an enhanced recombination, back reaction of photogenerated electrons and corrosion of metal NPs by the electrolyte.[148-154] Qi et al. has succeeded in fabricating highly efficient plasmon-enhanced DSCs using core-shell ($Ag@TiO_2$) nanostructures.[154] They had used Ag as core and TiO_2 as thin (about 2 nm) shell.

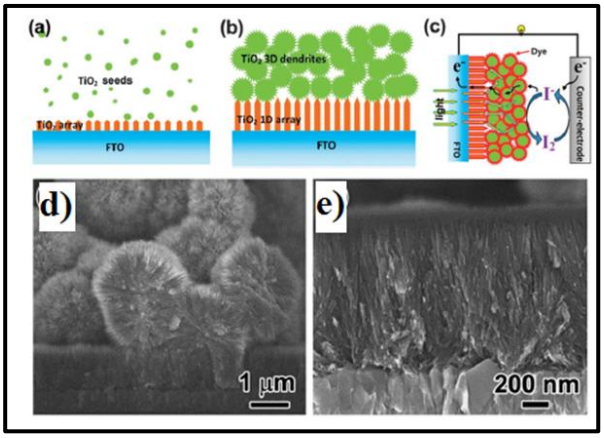

Fig. 45 Schematic of one step synthesis of bilayer formation (**a,b &c) a)** formation of TiO_2 seeds on FTO **b**) growth and assembly of 1D nanowire and 3D nanostructures **c)** bilayer photoanode of DSCs **d**) Magnified SEM image of 3D dendritic nanostructure **e)** SEM image of bilayer photoanode.[148]

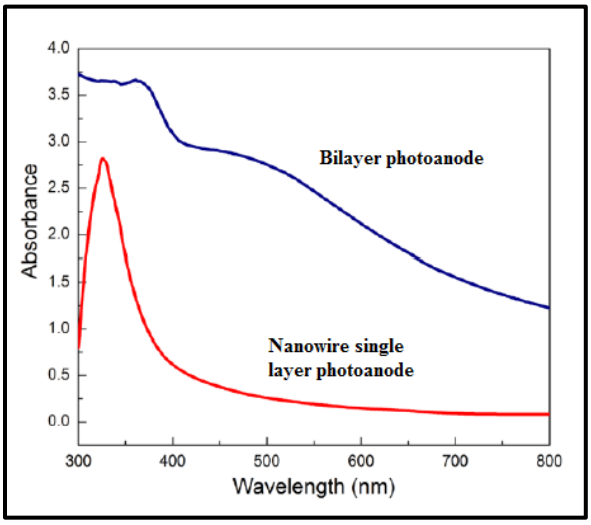

Fig.46 UV-Vis spectra of photoanodes with nanowire single layer and bilayer.[148]

The shell covering over metal NPs resulted in a reduced recombination and back reaction. Moreover it would also protect metal NPs from corrosion by electrolyte. The incorporation of 0.1 wt.% Ag@TiO_2 in thin photoanode provided increase in efficiency from 7.8% to 9.0%.

Further rod-like Ag and Au can also be utilized for developing highly efficient plasmon-enhanced DSCs. Longitudinal plasmon absorption of rod-like nanostrutures can be tuned by controlling the aspect ratio of the rod.[155-157] Chang et al. used Ag_2S-encapsulated Au nanorods (AuNR@AgS) in DSCs to enhance performance photocurrent at longer wavelength.[158] A 37.6% increment in photocurrent was observed at 600-720 nm range for AuNR@AgS incorporated photoanode. A power conversion efficiency about 7.1 % obtained for AuNR@AgS incorporated (11 µm thick) photoanode against 5.8% efficient TiO_2 alone photoanode DSCs.

6.4 1D-3D nanostructured rutile TiO_2 bilayer photoanodes

The highest efficiency for DSCs reported for rutile TiO_2 photoanode with a bilayer structure consisting of one-dimensional (1D) nanowire as underlayer and three-dimensional dendritic microsphere as top layer was 7.2%.[159] The vertically aligned 1D nanowires as bottom layer exhibited high photoinjected collection efficiency, fast electron transport and long electron diffusion length. The top layer of TiO_2 dendritic nanostructure with 1-3 µm diameters provided high specific surface area and in-turn high dye loading and light scattering.

The above favorable factors result in efficient bilayer DSCs. The one-step hydrothermal synthesis was used to fabricate photoanode where a mixture of titanium tetraisopropoxide (TTIP) and cetyltrimethylammonium bromide (CTAB) together with ethylene glycol (EG) was used for hydrothermal treatment. The FTO was kept in a Teflon-lined autoclave with the conducting side facing up. The formation of the bilayer is explained in **Fig. 45**. The size and morphology nanostructures can be adjusted by varying $TTIP_{aq}$/EG ratio. A fill-factor of 68% and J_{sc} of 14.51 mA cm^{-2} were obtained for best performing cells. The UV-Vis spectra reveal the pronounced light scattering effect exhibited by the bilayer photoanode (**Fig. 46**).

6.5 Quintuple-shelled SnO_2 hollow microsphere as light scattering layer

The SnO_2 has two major advantages over TiO_2 as DSC photoanode material: 1) it possesses a wider band-gap (3.8 eV), and 2) dye degradation is minimal because it creates fewer oxidative holes in its valence band under UV illumination. However the power conversion efficiency is limited for SnO_2-based DSCs due to following reasons:

1) a 300 mV positive shift in conduction band with respect to TiO_2 encourages interfacial recombination.
2) a lesser adsorption of dyes with acidic carboxylic groups.

Dong et al. reported a power conversion efficiency of 9.53% with quintuple-shelled SnO_2 hollow microsphere with closed exterior double walls (5S-SnO_2-HMs-CDS) as a light scattering layer.[160] The alkali-treated carbonaceous microspheres used as templates for synthesis of 5S-SnO_2-HMs-CDS. The efficiency increased by 30.7% when 5S-SnO_2-HMs-CDS with high light reflectance (%) was used as overlayer on P25 layer.

6.6 Multi-stack dye solar cells

Marco et al. engineered a photoanode with a combination of three mesoporous stacks made of different sized nanorods.[161] In this approach, the bottom layer consisted of small nanorods capable of excellent dye adsorption; an intermediate layer of nanorods with a high aspect ratio that ensured good electron transport and an upper layer consisting of large nanorods which guaranteed superior light scattering. These favorable conditions effectively contributed to a higher efficiency of 10.23% for the DSC. The thickness of the multi-stacked film was about 17 mA high current density of 18.10 mA cm^{-2} and a V_{oc} of 0.81 V were obtained for the three-layered cell.

7. Conclusions

Light scattering is an effective approach to enhance light absorption in a DSC photoelectrode. In general light scattering in DSCs is achieved in three ways: 1) mixing large particles with nanocrystalline TiO_2 slurry; 2) placing large particles as overlayer on TiO_2 photoelectrode film (double layer structure); 3) single layer of dual function materials. Theoretically increase in film thickness would enhance optical absorption of light. But the maximum allowed thickness of DSC photoanode film is limited by electron diffusion length. The first approach mentioned

CREATED USING THE RSC ARTICLE TEMPLATE (VER. 3.0) - SEE WWW.RSC.ORG/ELECTRONICFILES FOR DETAILS

ARTICLE TYPE www.rs

above would lead to decrease in internal surface area of the photoelectrode film. The additional overlayer for light scattering would retain internal surface area; however, the light is reflected only once. Dual function materials such as hierarchical 3D nanostructures provide both internal surface area and multiple reflections of incident light. The inclusion of scattering layer in DSCs would make it opaque that restrict the use of DSCs building-integrated photovoltaic applications. However, this can be sorted out by using photonic crystal as light scattering layer in DSC which makes it transparent to some extent. Commercializing DSC at low cost is one of the challenging tasks in solar energy conversion scenario. Inclusion of light scattering layer has become a common practice in the fabrication of high performance DSCs. Minimizing the thickness of active layer is highly recommended which would reduce recombination and usage of costly commercial dyes (~ $300/g). The diffused reflectance of NT and NS aggregate is around 80% at visible region. The microplate nanostructure has shown a better reflectance of about 80-90%. But these have a lower surface area which will limit the PV performance of DSCs. We saw that optimization of haze factor by adding light a scattering layer is also important criterion for obtaining best PV performance in DSCs.

Table 3 summarizes effect of different nanostructures for light scattering in DSCs.

Table 3. Different nanostructures as scattering layer and their impact in DSCs performance.

Nanostructures as scattering layer	Current density	Efficiency (η)	Increment in efficiency (in percentage)
Large spherical TiO_2 particles (with diameter ~ 400 nm)	21 mA cm^{-2}	11.1%	52%*
TiO_2 nanospindles	16.4 mA cm^{-2}	8.3%	43%
Nano-embossed hollow spherical TiO_2	15.8 mA cm^{-2}	9.43 %	21%
CeO_2 nanoparticles with diameter ~ 400 nm	19.3 mA cm^{-2}	8.6%	17.8%
Quintuple-shelled SnO_2 microsphere	20.1 mA cm^{-2}	9.53%	30.7%#
Multi-stacked DSCs	18.1 mA cm^{-2}	10.23%	40.29%$

*** $ # Here 7.29% is taken as efficiency of a standard P25 photoanode DSC.**

It clearly depicts that spherical nanoparticles with 400 nm diameter as light scattering layer show superior performance among others. Only major nanostructures that could provide considerable increment in efficiency are only listed in **Table 3**.

Multi-stacked DSCs also show superior PV performance compared to single and double layer DSCs. But the thickness of DSCs exceed more than 15μm (i.e. thicker solar cells) for the best performing solar cell. The spherical TiO_2 aggregate with nanotubes, nanorods and nanosheets as building units exhibits better electron transport property without giving up the internal surface area and light scattering. Designing TiO_2 tailored aggregates such as nanorod aggregate, nanosheet aggregate and nanotube aggregate with high surface area and light scattering capability as dual functional materials in DSCs would be a viable model for obtaining highly efficient DSCs.

Acknowledgement

The authors thank the Ministry of New and Renewable Energy, Govt. of India for financial assistance.

References

1 M. Grätzel, *Nature*, 2001,**414** , 338 .
2 A. Yella, H. W. Lee, H. N. Tsao, C. Yi, A. K. Chandiran, M. K. Nazeeruddin, E. W. G. Diau, C. Y. Yeh,S. M. Zakeeruddin, and M. Gratzel, *Science*, 2011, **334**,629.**b)**S.Mathew,A.Yella,P.Gao,R.H.Baker,B.F.E. Curchod,N.A.Astani,I.Tavernelli,U.Rothlisberger,M.K. Nazeeruddin and M.Grätzel, *Nature Chemistry*,2014 **6**, 242.
3 N. N. Bwana, *Nano. Res.*, 2008, **1**, 483.
4 K. H. Yu, J. H. Chen, *Nanoscale Res. Lett.*, 2009, **4**, 1.
5 S. Ramakrishna, R. Jose, P. S. Archana, A. S. Nair, R. Balamurugan, J. Venugopal, and W. E. Teo, *J. Mater. Sci.*, 2010, **45**, 6283.
6 A. Hagfeldt, G. Boscholo, L. Sun, L. Kloo, and H. Pettersson, *Chem. Rev.*, 2010, **110**, 6595.
7 Y.Chiba, A. Islam, Y. Watanabe, R. Komiya, N. Koide, and L. Han, *Jpn. J. Appl. Phys.***,** 2006, **45**, L638.
8 M.Grätzel, J. R. Durrant, in *Series on Photoconversionof Solar Energy* Vol. 3 (Eds: Mary D Archer & Arthur J), Imperial College Press, Nozik 2008, Ch 8. **b)** A. Listorti , B.O'Regan and J.R. Durrant, *Chem.Mater.*, 2011, **23**, 3381. **c)** M. Grätzel, *J. Photochem. Photobiol. C: Photochemistry Reviews*, 2003, **4** , 145.
9 M. Grätzel, *Inorg. Chem.*, 2005, **44**, 6841.
10 W. Kubo, T. Kitamura, K. Hanabusa, Y.Wada, and S. Yanagida, *Chem.Commun.*, 2002, **4**, 374.
11 A. Greijer, J. Lindgren, and A. Hagfeldt, *Photochem. Photobiol., A*, 2004, **164**, 23.
12 S. Nakade, W. Kubo, Y. Saito, T. Kanzaki, T. Kitamura, Y. Wada, and S. Yanagida, *J. Phys. Chem. B*, 2003, **107**,14244.

13 M. K. Nazeeruddin, A. Kay, I. Rodicio, R. Humphrey-Baker, E. Müller, P. Liska, N. Vlachopoulos, and M. Grätzel, *J. Am. Chem. Soc.*, 1993, **115**, 6382.

14 Y. Tachibana, J. E. Moser, M. Grätzel, D. R. Klug, and J. R. Durrant, *J. Phys. Chem.*,1996, **100,** 20056.

15 J. E. Moser, and M. Grätzel, *Chimia*, 1998, **52**, 160.

16 G. Benkö , J. Kallioinen, J. E. I. Korppi-Tommola, A. P. Yartsev, and V. Sundströ m, *J. Am. Chem. Soc.*, 2002, **124**, 489.

17 J. Kallioinen, G. Benkö , V. Sundströ m, J. E. I. Korppi-Tommola, and A. P. Yartsev, *J. Phys. Chem. B*, 2002, **106**, 4396.

18 G. Benkö , J. Kallioinen, P.Myllyperkiö , F.Trif, J.E.I. Korppi-Tommola, A.P Yartsev, and V.Sundströ m, *J. Phys. Chem. B*, 2004, **108**, 2862.

19 K. Schwarzburg, R. Ernstorfer,S. Felber, and F.Willig, *Coord. Chem.Rev.*, 2004, **248**, 1259.

20 A. Hagfeldt, S. E. Lindquist, and M.Grätzel, *Sol. Energy Mater. Sol.Cells*,1994, **32**, 245.

21 A. Hagfeldt, and M.Grätzel, *Chem. Rev.*,1995, **95**, 49.

22 A. Stanley, and D.Matthews, *Aust. J. Chem.*,1995, **48**, 1294.

23 B O'Regan, J.Moser, M.Anderson, and M.Grätzel, *J. Phys. Chem.*,1990, **94**, 8720.

24 S. Sö dergren, A. Hagfeldt, J. Olsson, and S. E. Lindquist, *J Phys. Chem.*,1994, ***98***, 5552.

25 A. Solbrand, H. Lindströ m, H. Rensmo, A. Hagfeldt, S. E. Lindquist, and S. Sö dergren, *J. Phys. Chem. B*,1997, **101**, 2514.

26 N. Kopidakis, E. A. Schiff, N. G. Park, J. van de Lagemaat, and A. Frank, *J. Phys. Chem. B* **2000**, *104*, 3930.

27 D. Nistèr, K. Keis, S. E. Lindquist, and A. Hagfeldt, *Sol. Energy Mater.Sol. Cells* , 2002, **73**, 411.

28 F. Cao, G. Oskam, and P. C. Searson, *J. Phys. Chem.*, 1996, ***100***, 17021.

29 L. Dloczik, O.Ileperuma, I. Lauermann, L. M. Peter, E. A. Ponomarev, G. Redmond, N. J. Shaw, and I. Uhlendorf, *J. Phys. Chem. B*,1997, **101**, 10281.

30 A. Hauch, and A. George, *Electrochim. Acta* , 2001, **46**, 3457.

31 T. Daeneke, T. H. Kwon, A. B. Holmes, N. W. Duffy, U. Bach and L. Spiccia, *Nat. Chem.*,2011,**3**, 211.

32 S. Hattori, Y. Wada, S.Yanagida, and S.Fukuzumi, *J. Am.Chem. Soc.*,2005, **127**, 9648.

33 T. C. Li, A. M. Spokoyny, C. She,O. K. Farha, C. A. Mirkin,T. J. Marks, and J. T. Hupp, *J. Am. Chem. Soc.*, 2010, **132**, 4580.

34 J. J. Nelson, T. J. Amick, and C. M. Elliott, *J. Phys. Chem. C*, 2008, **112**, 18255.

35 B. M. Klahr, and T. W. Hamann, *J. Phys. Chem. C*, 2009, **113**,14040.

36 M. K. Kashif, J. C. Axelson, N. W. Duffy, C. M. Forsyth, C. J. Chang, J. R. Long, L. Spiccia, and U. Bach, *J. Am.Chem. Soc*., 2012, **134**, 16646.

37 Q. Zhang, D. Myers, J. Lan, S. A. Jenekhe, and G.Cao, *Phys. Chem. Chem. Phys.*, 2012, **14**, 14982.

38 M. A. Anderson, M. J. Geiselmann, and J. Q. Xu, *J. Membr. Sci.*,1988, **39**, 243.

39 B. O'Regan, J. Moser, M. Anderson, and M. Grätzel, *J. Phys. Chem.*, 1990, **94**, 8720.

40 M. Grätzel, *Heterogeneous Photochemical Electron Transfer*, CRC Press, Baton Rouge, FL, 1988.

41 R. Konenkamp, R. Henninger, and P. Hoyer, *J. Phys. Chem.*, 1993, **97**, 7328.

42 R. Konenkamp, and R. Henninger, *Appl. Phys. A*, 1994, **58**, *87.*

43 G. Hodes, I. D. J. Howell, and L. M. Peter, *J. Electrochem. Soc.*, 1992, **139**, 3136**.**

44 A. Hagfeldt, U. Bjorksten, and S. E. Lindquist, *Sol. Energy Mat. Sol. Cells*, 1992, **27**, 293.

45 R.Vogel, P. Hoyer, and H.Weller, *J. Phys. Chem.*,1994, **98**, 3183.

46 A. Usami, *Chem. Phys. Lett.*, 1997, **277,** 105.

47 C. J. Barbè, F. Arendse, P. Comte, M. Jirousek, F. Lenzmann, V. Shklover, and M. Grätzel, *J. Am. Ceram. Soc.*, 1997, **80**, 3157.

48 J. Ferber, and J. Luther, *Sol. Energy Mat.Sol. Cells*, 1998, **54**, 265.

49 J.Ferber, Spektrale und winkelabhangige Charakterisierung stark streuender Schichten, Thesis, University of Freiburg, 1994.

50 S .Chandrasekhar, *Radiative Transfer*, Dover, New York, 1960.

51 G. Rothenberger, P. Comte, and M. Grätzel, *Sol. Energy Mat. Sol. Cells***,**1999, **58**, 321.

52 Y.Tachibana, K. Hara, K. Sayama, and H. Arakawa, *Chem. Mater.*, 2002**, 14,** 2527.

53 S. Hore, P. Nitz, C.Vetter, C. Prahl, M. Niggemannb, and R. Kernab, *Chem. Commun*., 2005, **15**, 2011.

54 C. L. Huisman, J. Schoonman, and A. Goossens, *Sol. Energy Mater. Sol. Cells*, 2005, **85**, 115.

55 S. Nishimura, N. Abrams, B. A. Lewis, L. I. Halaoui, T. E. Mallouk, K. D. Benkstein, J. van de Lagemaat, and A. J. Frank, *J. Am. Chem. Soc.*, 2003, **125**, 6306.

56 A. Ishimaru, in *Wave Propagation and Scattering in Random Media*, Academic Press, New York, 1978.

57 G.Yang, J. Zhang, P.Wang, Q. Sun, J. Zheng, and Y. Zhu, *Curr. Appl. Phy.*, 2011**, 11**, 37.

58 Y. Sanehira, S. Uchida, *Kagaku Kogyo*, 2004, **55**, 796.

59 J. B. Baxter, E. S. Aydil, *Sol. Energy Mater. Sol. Cells*, 2006, **90** , 607.

60 B. Tan, and Y. Wu, *J. Phys. Chem. B*, 2006**, 110**, 15932.

61 P. Joshi, L. Zhang, D. Davoux, Z. Zhu, D. Galipeau, H. Fong, and Q. Qiao, *Energy Environ. Sci.*, 2010, **3**, 1507.

62 H. Van, *Light Scattering by Small particles*, John Wiley & Sons, New York, 1957.

63 Y. Dzenis, *Science*, 2004, **304**, 1917.

64 Z-S.Wang, H. Kawauchi, T. Kashima, and H. Arakawa, *Coord. Chem. Rev.*,2004, **248**, 1381.

65 S. Hore, C.Vetter, R. Kern, H. Smit, and A. Hinsch, *Sol. Energy Mater. Sol. Cells*, 2006, **90**, 1176.

66 J-K. Lee, B-H. Jeong, S. J. Y-G. Kim,Y-W. Jang, S-B. Lee, and M.-R. Kim *J. Ind. Eng. Chem.*, 2009,**15** , 724.

67 C-S. Chou, M-G. Guo, K-H. Liu, and Y-S. Chen, *Appl. Energ.*, 2012, **92**, 224.

68 L.Yanga, L. Lina, J. Jia , X. Xiaoa, and X. L. X. Zhoua, *J. Power Sources*, 2008, **182**, 370.

69 K. Nakayama, T. Kubo, and Y. Nishikitani, *Jpn. J. Appl. Phys*., 2008, **47**, 6610.

70 A. M. Bakhshayesha, M. R. Mohammadia, H. Dadara, and D. J. Fray, *Electrochim. Acta*., 2013, **90**, 302.

71 M. R. Mohammadi, D. J. Fray, and A. Mohammadi, *Micropor. Mesopor. Mat.*, 2008**, 112**, 392.

72 Y. Qiu, W. Chen, and S.Yang, *Angew. Chem. Int. Ed.*, 2010, **49**, 3675.

73 S. Chuangchote, T. Sagawa, and S. Yoshikawa, *Appl. Phys. Lett.*, 2008, **93**, 033310.

74 P. Zhu, A. S. Nair, S.Yang, S. Peng, and S. Ramakrishna, *J. Mater. Chem*., 2011, **21,** 12210.

75 S. Nair, Y. Yang, P. N. Zhu, and S. Ramakrishna, *Chem.Commun*.,2010, **46**, 7421.

76 S. Y. Yang, P. N. Zhu, A. S. Nair, and S. Ramakrishna, *J. Mater.Chem.*, 2011, **21**, 6541.

77 K. Mukherjee, T. H. Teng, R. Jose, and S. Ramakrishna, *Appl. Phys.Lett***.,**2009, **95**, 012101.

78 G. Zhu, L. Pan, J.Yang, X. Liu, H.Sun, and Z.Sun, *J. Mater. Chem.*, 2012, **22**, 24326.

79 H-J. Koo, Y. J. Kim, Y. H. Lee, W. I. Lee, K. Kim, and N-G.Park, *Adv. Mater.*, 2008, **20**, 195.

80 W. Shao, F. Gu, L. Gai, and C. Li, *Chem. Commun.*, 2011, **47**, 5046.

81 Y. Li, T. Sasaki, Y. Shimizu, and N. Koshizaki, *Small* , 2008, **4**, 2286.

82 Y. Li, T. Sasaki, Y. Shimizu, and N. Koshizaki, *J. Am. Chem. Soc.*, 2008, **130**, 14755.

83 Y. Zeng, X. Wang, H. Wang, Y. Dong, Y. Ma , and J. Yao, *Chem.Commun*., 2010, **46**, 4312.

84 H. Jiang, J. Hu, C. Li, F. Gu, and J. Ma, *Cryst.Eng.Comm.*, 2010, **12**, 1726.

85 W. Peng, and L. Han, *J. Mater. Chem.*,2012, **22**, 20773.

86 S. Nishimura, N. Abrams, B. Lewis, and L. Halaoui, *J. Am. Chem. Soc.*, 2003**, 125**, 6306.

87 L. Halaoui, N. Abrams, and T. Mallouk, *J. Phys. Chem. B*, 2005, **109**, 6334.

88 A. Mihi, M. E. Calvo, J. A. Anta, and H. Míguez, *J. Phys. Chem. C*, 2008, **112**, 13.

89 S. Colodrero, A. Mihi, L. Haggman, M. Ocana, G. Boschloo, A. Hagfeldt, and H. Míguez, *Adv. Mater*.,2009, **21**, 764.

90 K. Sakoda, *Opt. Express* ,1999, **4**, 167.

91 D. Mittleman, J. Bertone, P. Jiang, K. Hwang, and V. J. Colvin, *Chem.Phys.*, 1999, **111**, 345.

92 R. Rengarajan, D. Mittleman, C. Rich, and V. Colvin, *Phys. Rev. E*, 2005, **71**, 15968.

93 A. Mihi, and H. Míguez, *J. Phys. Chem. B*, 2005, **109**, 15968.

94 (a) R. J. Carlson, S. A. Asher, *Appl. Spectroscopy*, 1984, **38**, 297. (b) P. L. Flaugh, S. E. O Donnell, and A. S. Asher, *Appl. Spectroscopy*, 1984, **38**, 847.

95 S. Nishimura, N. Abrams, B. A. Lewis, L. I. Halaoui, T. E. Mallouk, K. D. Benkstein, J. van de Lagemaat, and A. J. Frank, *J. Am. Chem. Soc.*, 2003, **125**, 6306.

96 A.Mekis, J.C.Chen, I.Kurland, S.Fan, P.R.Villeneuve, a nd J. D. Joannopoulos, *Phys. Rev. Lett.*, 1996, **77**, 3787.

97 B.W. Batterman, and H. Cole, *Rev. Mod. Phys*., 1964, **36**, 681.

98 J. E. G. J. Wijnhoven, and W. L. Vos, *Science*, 1998, **281**, 802.

99 B. T. Holland, C. F. Blanford, and A. Stein, *Science*, 1998, **281**, 538.

100 B.T.Holland,C.F.Blanford, T.Do, and A.Stein, *Chem. Mater*., **1999**, *11*,795.

101 A. Richel, N. P. Johnson, and D.W. McComb, *Appl. Phys. Lett***.,** 2000, **76**,1816.

102 M. E.Turner, T. J. Trentler, and V. L. Colvin, *Adv. Mater*. 2001, **13**, 180.

103 Y. A.Vlasov, X.-Z. Bo, J. C. Sturm, and D. J. Norris, *Nature*, 2001, **414**,289.

104 Schroden, R. C. Al-Daous, M. Blanford, and C. F. Stein, *Chem. Mater***.,** 2002, **14**, 3305.

105 P. Jiang, J. F. Bertone, K. S. Hwang, and V. L. Colvin, *Chem. Mater.*, 1999, **11**, 2132.

106 H. Kishimoto, K. Takahama, N. Hashimoto, Y. Aoi, and S. Deki, *J. Mater.Chem.*, 1998**, 8,** 2019.

107 S. Deki, and Y. Aoi, *J. Mater. Res.*, 1998, **13**, 883.

108 K. Koumoto, S. Seo,T. Sugiyama, and W. S. Seo, *Chem. Mater.*, 1999, **11,** 2305.

109 K. Shimizu, H. Imai, H. Hirashima, and K. Tsukuma, *Thin Solid Films*, 1999, **351**, 220.

110 Imai, H. Takei, Y. Shimizu, K. Matsuda, and M. Hirashima, *J. Mater. Chem***.,** 1999, **9**, 2971.

111 S.Yamabi, and H. Imai, *Chem. Mater*., 2002, **14**, 609.

112 S. Nishimura, A. Shishido, N. Abrams, and T. E. Mallouk, *Appl. Phys. Lett.*, 2002, **81**, 4532.

113 A. Mihi, and H. Míguez, *J. Phys. Chem. B*, 2005, **109**, 15968.

114 S. Guldin, S. Huttner, M. Kolle, M. E. Welland, P. Müller-Buschbaum, R. H. Friend, U. Steiner, and N. Tètreaul, *Nano Lett*., 2010, **10**, 2303.

115 H.Yu, Y. Bai, X. Zong, F.Tang, G. Q. Max Lu, and L.Wang, *Chem. Commun.*, 2012, **48**, 7386.

116 F. H. Scholes, A. E. Hughes, S. G. Hardin, P. Lynch, and P. R. Miller, *Chem. Mater.*, 2007, **19**, 2321.

117 S. C. Choi, H. S. Lee, S. J. Oh , and S. H. Sohn, *Phys. Scr*., 2012, **85**, 025801.

118 S. J. Seo, and S. H. Sohn, *Mater. Lett*., 2010, **64** 1264.

119 E. M. Kaidashev, M. Lorenz, H. von Wenckstern, A. Rahm, H. C. Semmelhack, K. H. Han, G. Benndorf, C. Bundesmann, H. Hochmuth, and M. Grundmann, *Appl. Phys. Lett.*, 2003, **82**, 3901.

120 T. Dittrich, E. A. Lebedev, and J. Weidmann, *Phys. Status Solidi A: RRN*, 1998, **165**, R5.

121 T. P. Chou, Q. F. Zhang, G. E. Fryxell, and G. Z. Cao, *Adv.Mater*., 2007, **19**, 2588.

122 D. Jezequel, J. Guenot, N. Jouini, and F. Fievet, *J. Mater. Res.*, 1995, **10**, 77.

123 E. W. Seelig, B. Tang, A. Yamilov, H. Cao, and R. P. H. Chang, *Mater. Chem. Phys.*, 2003, **80**, 257.

124 J. F. Qian, P. Liu, Y. Xiao, Y. Jiang, Y. L. Cao, X. P. Ai, and H. X. Yang, *Adv. Mater.*, 2009, **21**, 3663.

125 Q. F. Zhang, T. R. Chou, B. Russo, S. A. Jenekhe, and G. Z. Cao, *Angew. Chem., Int. Ed*., 2008, **47**, 2402.

126 N. Memarian, I. Concina, A. Braga, S. M. Rozati, A. Vomiero and G. Sberveglieri, *Angew. Chem., Int. Ed.*, 2011, **50**, 12321.

127 Y. J. Kim, M. H. Lee, H. J. Kim, G. Lim, Y. S. Choi, N. G. Park, K. Kim, and W. I. Lee, *Adv. Mater*., 2009, **21,** 3668.

128 D. H. Chen, F. Z. Huang, Y. B. Cheng, and R. A. Caruso, *Adv.Mater.*, 2009, **21**, 2206.

129 F. Sauvage, D. H. Chen, P. Comte, F. Z. Huang, L. P. Heiniger,Y. B. Cheng, R. A. Caruso, and M. Gratzel, *ACS Nano*, 2010, **4**, 4420.

130 M. Nedelcu, S. Guldin, M. C. Orilall, J. Lee, S. Huttner, E. J. W.Crossland, S. C. Warren, C. Ducati, P. R. Laity, D. Eder,U. Wiesner, U. Steiner, and H. J. Snaith, *J. Mater. Chem.*, 2010, **20**, 1261.

131 Z. Peining, W.Yongzhi, M. V. Reddy, A. S. Nair, P. Shengjie, N. Sharma, V. K. Peterson, B.V. R. Chowdari, and S. Ramakrishna, *RSC Adv.*, 2012, **2**, 5123.

132 P. Zhu, M. V. Reddy, Y. Wu, S. Peng, S. Yang, A. S. Nair, K. P. Loh, B. V. R. Chowdari and S. Ramakrishna ,*Chem. Commun*., 2012, **48**, 10865.

133 Z. H. Liu, X. J. Su, G. L. Hou, S. Bi, Z. Xiao, and H. P. Jia, *J. Power Sources*, 2012, **218**, 280.

134 Z. Liu, X. Su, G. Hou, S. Bi, Z. Xiao, and H. Jia, *Nanoscale*, 2013, **5**, 8177.

135 A. L. Aden, and M. Kerker, *J. Appl. Phys.* 1951, **22**, 1242.

136 R.W. Johnson, E. S.Thiele, R. H. French, *Tappi J.* 1997, **80**, 233.

137 W. P. Hsu, R.Yu, and E. Matijevic, *J. Colloid Interface Sci.*, 1993, **156,** 56,

138 S. Son ,S. H. Hwang , C. Kim , J. Y.Yun, and J. Jang, *ACS Appl. Mater. Interfaces*, **2013**, *5 ,4815.*

139 R. Watanabe, T. Yokoi, E. Kobayashi, Y. Otsuka, A. Shimojima, T. Okubo, and T. Tatsumi, *J. Colloid Interface Sci.*, 2011, **360**, 1.

140 Y. Takano, K. N. Liou, *Appl. Opt*., **2010**, *49*, 3990.

141 L. Zhao, J. Li, Y. Shi, S. Wang, J. Hu, B. Dong, H. Lu , and P. Wang, *J. Alloys Compd.*, **2013**,*575*,168.

142 P. Mulvaney, *Langmuir*, 1996, **12**, 788 .

143 F. Fabregat-Santiago, J. Bisquert, L. Cevey, P. Chen, M. Wang, S. M. Zakeeruddin, and M. Grätzel , *J. Am. Chem. Soc.*, 2009, **131** , 558 .

144 I.-K. Ding, N. Tetreault, J. Brillet, B. E. Hardin, E. H. Smith, S. J. Rosenthal, F. Sauvage, M. Gratzel, and M. D. McGehee, *Adv. Funct.Mater.*, 2009, **19** , 2431 .

145 H. J. Snaith, R. Humphry-Baker, P. Chen, I. Cesar, S. M. Zakeeruddin, and M. Grätzel, *Nanotechnology*, 2008, **19** , 424003 .

146 H. A. Atwater, and A. Polman, *Nat. Mater*., 2010 **, 9** , 205.

147 I-K. Ding, J. Zhu, W. Cai, S-J. Moon, N. Cai, P.Wang, S. M. Zakeeruddin, M. Grätzel, M. L. Brongersma, Y. Cui, and M. D. McGehee, *Adv. Energy Mater*., 2011, **1**, 52.

148 M.Ihara, K.Tanaka, K.Sakaki, I.Honma, K.Yamada, *J. Phys.Chem. B*, 1997, **101**, 5153.

149 K.Ishikawa, C.J.Wen, K.Yamada,T. Okubo, *J. Chem. Eng. Jpn.*, 2004, **37**, 645.

150 C. Hagglund, M. Zach, B. Kasemo, *Appl. Phys. Lett.*, 2008, **92**, 013113.

151 S.D. Standridge,G.C. Schatz, J.T. Hupp, *J. Am. Chem. Soc.*, 2009, **131**, 8407.

152 G. Zhao, H. Kozuka, T. Yoko, *Sol. Energy Mater. Sol. Cells*,1997,**46**, 219.

153 C. Wen, C. Ishikawa, M. Kishima, K.Yamada, *Sol. Energy Mater. Sol. Cells*, 2000, **61**, 339.

154 J. Qi, X. Dang, P.T. Hammond and A.M. Belcher, *ACS Nano*, 2011, **5**, 7108.

155 X. S. Kou, S. Z. Zhang, C. K. Tsung, Z. Yang, M. H. Yeung, G. D. Stucky, L. D. Sun, J. F. Wang and C. H. Yan, *Chem.Eur.J.*, 2007, **13**, 2929.

156 W. Ni, X. Kou, Z. Yang and J. F. Wang, *ACS Nano*, 2008, **2**, 677.

157 J. Pèrez-Juste, I. Pastoriza-Santos, L. M. Liz-Marzàn and P. Mulvaney, *Coord. Chem. Rev.*, 2005, 249, 1870.

158 S. Chang, Q.Li, X. Xiao, K.Y. Wonga and T.Chen, *Energy Environ. Sci.*, 2012,**5**, 9444.

159 Z. Sun, J. H. Kim, Y. Zhao, D. Attard and S. X. Dou, *Chem. Commun*., 2013,**49**, 966.

160 Z. Dong , H. Ren, C. M. Hessel, J. Wang, R. Yu, Q. Jin, M. Yang, Z. Hu, Y. Chen, Z. Tang, H. Zhao, and D. Wang, *Adv. Mater*., 2014, **26**,905.

161 L. D. Marco, M. Manca, R. Giannuzzi, M. R. Belviso, P. D. Cozzoli and G. Gigli, *Energy Environ. Sci.*, 2013, **6**,1791.

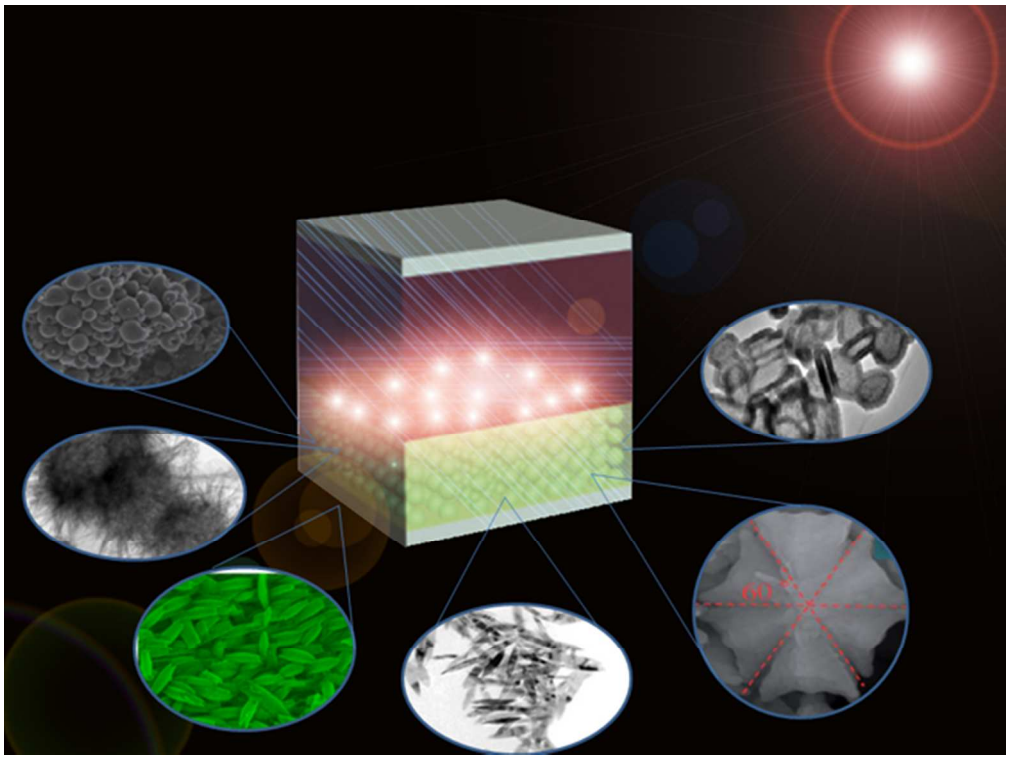

55x41mm (300 x 300 DPI)

A state-of-the-art review highlighting the theory, role and the materials of scattering layer in dye-sensitized solar cells.

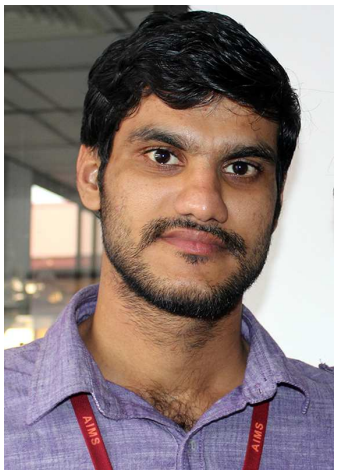

T.G. Deepak

Deepak completed his MSc degree in physics with specialization in Non-Conventional Energy from Mahatma Gandhi University, Kottayam, India. Currently he is a Junior Research Fellow at the Nanosolar Division of Amrita Center for Nanosciences, Kochi, Kerala, India. He works on photon/light management strategies for efficient dye-sensitized solar cells. His other areas of interest include quantum physics, nanotechnology for energy applications and philosophical implications of physics.

G.S Anjusree

Miss G. S. Anjusree received her M.Tech in Nanotechnology from Amrita Vishwa Vidyapeetham in 2012. She is currently a Senior Research fellow at Amrita Center for Nanosciences & Molecular Medicine at Kochi, Kerala, India. Her research interests are in electrospun anisotropic TiO_2 nanostructures for dye-sensitized solar cells/modules.

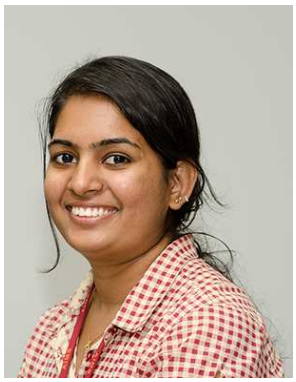

Sara Thomas

Miss Sara Thomas was a junior research fellow at Amrita Centre for Nanoscience & Molecular Medicine at Kochi, Kerala, India. She received M.Sc in Nanoscience and Nanotechnology from Bangalore University, India. She works on dye-sensitized solar cells.

T. A. Arun

Arun received his M.Tech Degree in Nanotechnology from Amrita Center for Nanosciences & Molecular Medicine, Amrita Vishwa Vidhyapeetham, Kerala, India and M.Sc. Physics from Mahatma Gandhi University, Kerala, India. His current research includes photoanode modification for dye-sensitized solar cells.

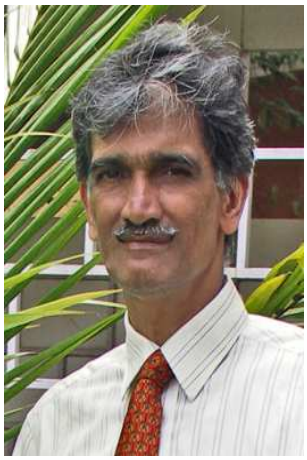

Dr. Shantikumar V Nair

Dr. Shantikumar V Nair is currently the Director of Amrita Centre for Nanosciences & Molecular Medicine at Kochi, Kerala, India. A graduate of IIT Bombay (Mumbai) in Metallurgical Engineering, he received his PhD from Columbia University, New York (1983). Prior to joining Amrita, he was a professor at the University of Massachusetts at Amherst. He is a recipient of the prestigious Presidential Young Investigator Award from the President of the United States (1986) and National Research Award from the Ministry of Science and Technology, Govt. of India (2011).

Dr. A. Sreekumaran Nair

Dr. A. Sreekumaran Nair is currently an Associate Professor at Amrita Centre for Nanosciences & Molecular Medicine at Kochi, Kerala, India. He did PhD (Chemistry) at Indian Institute of Technology (IIT) Madras (2006) and had postdoctoral trainings at University of Hyogo, Japan (JSPS fellow, 2006-2008) and Nanoscience and Nanotechnology Initiative at National University of Singapore (2008-2012), respectively. His current research interests include organic-inorganic nanohybrids for renewable energy, self-cleaning coatings and environmental remediation.